

# Sparse Tree-Based Aggregation for Time Series Regressions

Marie Corillon<sup>1</sup>, Stephan Smeekes<sup>1</sup>, and Ines Wilms<sup>1</sup>

<sup>1</sup>Department of Quantitative Economics, Maastricht University, The Netherlands

June 2, 2026

## Abstract

High-dimensional time series regressions are often regularized to produce sparse coefficients. We show that temporal aggregation provides a powerful alternative to reduce dimensionality in high-order autoregressions and mixed-frequency regressions. To this end, we propose StarTime (Sparse Tree-based Aggregation for Time Series), a convex penalization method that uses a temporal tree to arrange lags hierarchically from high to low frequency. StarTime then flexibly selects coefficients to be aggregated at possibly varying frequencies, sparse or a combination thereof. We provide new error bounds for StarTime, demonstrate improved estimation accuracy and recovery of aggregation and sparsity in simulations relative to benchmarks, and illustrate StarTime's relevance for financial and macroeconomic applications.

**Keywords.** Aggregation, forecasting, mixed-frequency data, penalization, time series

**JEL-Classification.** C22, C32, C55

## 1 Introduction

Forecasting financial and macroeconomic variables increasingly requires modeling dynamics that unfold across multiple time periods and temporal resolutions.

Daily realized volatility, for example, displays pronounced serial correlation, implying that current outcomes depend on a long history of past observations (see, e.g., [Corsi, 2009](#)). Besides, empirical research increasingly requires mixed-frequency settings where higher-frequency predictors forecast a lower-frequency response; the MIXed DATA Sampling (MIDAS) framework ([Ghysels et al., 2004](#)) forms a prominent example. In both examples, the persistence and frequency mismatch naturally lead to high-dimensional models with many highly correlated mixed-frequency regressors. In this paper, we propose the Sparse Tree-Based Aggregation for Time Series Regressions (*StarTime*) penalized estimator that addresses the dimensionality in such models through data-driven

temporal aggregation. It determines the sampling frequency at which lagged predictors enter the model, allowing for coefficients to be sparse, aggregated at varying lower frequencies, or both.

Time series are nowadays recorded at relatively fine temporal resolutions (e.g., daily financial or weekly macroeconomic series). Modeling such series with high-order autoregressions or mixed-frequency regressions quickly gives rise to the curse of dimensionality. First, strong serial dependence implies that predictive information may be distributed across many, potentially noisy lags. Second, in mixed-frequency regressions, the problem is further amplified by the frequency mismatches: A single lower-frequency observation corresponds to numerous higher-frequency predictors, each entering as a separate regressor. As the frequency mismatch widens – for example, in daily-to-quarterly rather than monthly-to-quarterly settings – the dimensionality can increase substantially.

Penalized estimators such as the Lasso and extensions have become popular to address dimensionality in (mixed-frequency) time series regressions (see e.g.; [Luo et al., 2025](#); [Babii et al., 2024](#); [Masini et al., 2023](#); [Hecq et al., 2022](#); [Babii et al., 2022](#); [Smeekes and Wijler, 2021](#); [Mogliani and Simoni, 2021](#)). These are particularly effective when the underlying model is sparse. Persistent and mixed-frequency environments, however, differ in important ways. When dynamics are smooth and distributed over time, the true lag structure may be dense rather than sparse with adjacent lags typically being highly correlated. As additional lags are included, the design matrix becomes increasingly collinear, undermining variable selection procedures that operate on individual coefficients. In such settings, penalized methods may overshrink lagged effects or select unstable subsets of lags, failing to capture the underlying temporal structure (see, e.g., [Zou and Hastie, 2005](#)).

Temporal aggregation provides an appealing alternative when dynamics are smooth and densely distributed over time. Work on the impact of temporal aggregation on time series has long been studied (e.g., [Veredas and Silvestrini, 2008](#); [Rossana and Seater, 1995](#); [Brewer, 1973](#); [Amemiya and Wu, 1972](#); [Tiao, 1972](#)). In finance, the Heterogeneous Autoregressive (HAR) model ([Corsi, 2009](#)) offers a prominent, popular example: It aggregates daily realized volatility into weekly and monthly components, motivated by investor heterogeneity across trading horizons. HAR-type models have demonstrated strong forecasting performance, often rivaling or outperforming more complex machine learning approaches such as the Lasso ([Chassot and Audrino, 2026](#)). Similarly, aggregation-based measures have been developed to mitigate microstructure noise in high-frequency financial data (e.g., [Bollerslev et al., 2006](#); [Todorov and Tauchen, 2012](#) ).

In macroeconomics, mixed-frequency models also commonly rely on aggregation schemes to align predictors sampled at different rates. MIDAS regressions ([Ghysels et al., 2004](#)) employ polynomial

distributed lags, while restricted MIDAS (Andreou, 2016) and bridge equations (Schumacher, 2016) impose shape restrictions or fixed weighting schemes to simplify estimation. These approaches have been widely adopted in macroeconomic and financial applications (Ghysels et al., 2007). While these aggregation-based methods effectively reduce noise and dimensionality, they typically require the aggregation scheme to be specified *a priori*. In practice, however, the appropriate temporal resolution may not be known in advance. This motivates the need for flexible procedures that determine the temporal aggregation structure in a data-driven way; we fill this gap in this paper.

In this paper, we propose *StarTime* (Sparse Tree-Based Aggregation for Time Series Regressions), a penalized estimation procedure designed to reduce dimensionality in autoregressive and mixed-frequency regressions through data-driven temporal aggregation. *StarTime* allows adjacent lags to share a common coefficient, thereby selecting the sampling frequency at which lagged effects enter the model. The estimator can produce sparse coefficients, temporally aggregated coefficients at varying lower frequencies, or a combination of both, enabling fully data-driven selection of the effective temporal resolution. To implement this idea, we leverage a temporal tree that reflects natural aggregation across frequencies. For each predictor, lags are arranged hierarchically from its highest available frequency (leaf nodes) toward progressively lower sampling frequencies (internal and root nodes). We embed this tree structure into the penalty of a convex optimization problem, encouraging nearby lags to fuse when supported by the data. When the underlying lag pattern varies smoothly, the procedure can aggregate adjacent lags and estimate identical coefficients. When finer resolution is warranted, it retains disaggregated lag-specific effects. Tree-based parameterizations have proven successful for high-dimensional regressions (Yan and Bien, 2021; Fu et al., 2025) and graphical models (Wilms and Bien, 2022); we adapt and extend these ideas to high-order autoregressions and mixed-frequency time-series regressions.

Figure 1 illustrates *StarTime*'s ability to recover temporally aggregated lag structures in a data-driven manner. We consider an autoregressive model of order 20 for the log-transformed realized variance of Apple Inc. (AAPL) and compare the estimated coefficients returned by the HAR, Lasso, and *StarTime*. The HAR returns a parsimonious coefficient structure by *a priori* specifying aggregation at the daily, weekly and monthly lag frequency. The Lasso selects individual lags in a data-driven yet scattered and difficult-to-interpret manner; its performance relative to the HAR model has been mixed (e.g., Zhang et al., 2024; Christensen et al., 2023; Audrino et al., 2020; Audrino and Knaus, 2016). *StarTime* uncovers a coherent aggregation structure that closely aligns with the economically-motivated HAR specification, particularly when combined with a 'post-selection' de-biasing step (Post versus Simple *StarTime*; further discussed in Section 3). In

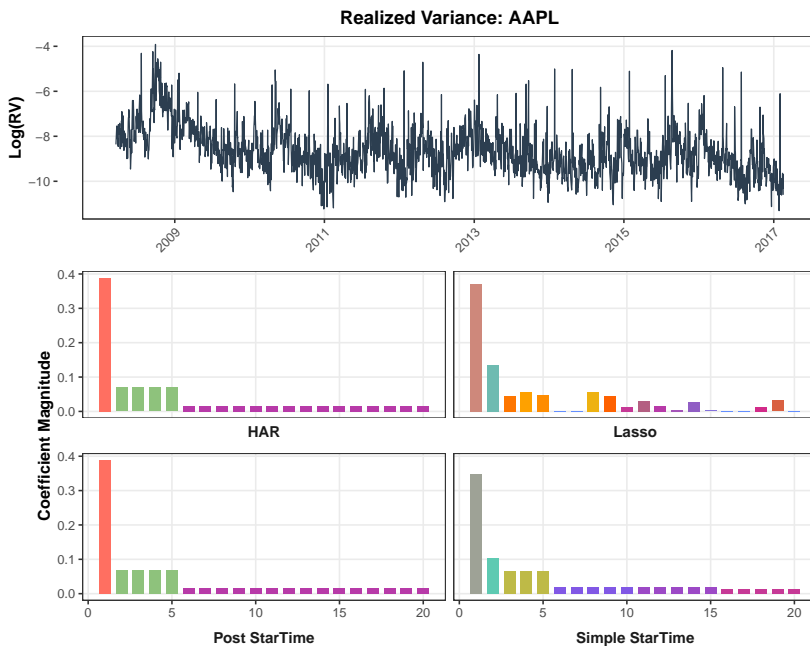


Figure 1: Top: Log-transformed realized variance for Apple Inc. (AAPL) from March 20, 2008 to February 17, 2017. Middle and Bottom: Estimated coefficients for the HAR (middle left), Lasso (middle right), and StarTime (bottom). Identical coefficient values are displayed in the same color.

contrast to the HAR, StarTime uncovers the temporal aggregation structure among the lags in a fully data-driven manner, making it broadly applicable across diverse empirical settings.

We derive new error bounds for StarTime to guarantee consistency for prediction and estimation under Near-Epoch Dependence (NED) assumptions. We extend the results for independent and identically distributed (IID) data in [Yan and Bien \(2021\)](#) to time series settings in typical econometrics applications that are characterized by non-Gaussianity, serial dependence, heteroskedasticity, and heavy tails. We hereby leverage the theoretical framework developed in [Adamek et al. \(2023\)](#). Monte Carlo simulations demonstrate good performance of StarTime in high-order autoregressive and mixed-frequency settings, particularly when the true lag structure is dense but smooth. Finally, we illustrate the empirical relevance of StarTime in financial and macroeconomic applications.

The remainder of the paper is organized as follows. Section 2 introduces the modeling framework and the tree-based aggregation mechanism. Section 3 presents our penalized estimator and its algorithmic implementation. Section 4 establishes the theoretical properties of our estimator. Section 5 reports simulation results for autoregressive and mixed-frequency settings, and Section 6 provides empirical applications. Section 7 concludes.

## 2 Temporal Aggregation in Time Series Regressions

In Section 2.1, we introduce our general model set-up for mixed-frequency regressions. In Section 2.2, we propose a tree-based parametrization structure for temporal aggregation in such regressions.

### 2.1 The Mixed-Frequency Regression Model

We consider a general linear regression model for mixed-frequency time series, where the explanatory variables are observed at higher (or equal) frequencies than the response. Let  $y_{mt}$  ( $t = 1, \dots, T$ ) be the response at time  $mt$  and let  $x_\tau^{[i]}$  be the  $i$ th ( $i = 1, \dots, D$ ) explanatory variable at time  $\tau$ . For convenience, let the first variable ( $i = 1$ ) be observed at the highest frequency with  $m$  recording its frequency mismatch with the response; high-frequency variable  $i = 1$  is observed  $m$  times per low-frequency period of the response (e.g., for quarterly/monthly data  $m = 3$ ). Analogously,  $m_i \geq 1$  denotes the frequency mismatch of variable  $i$  relative to the first (by construction  $m_1 = 1$ ).

The model is given by

$$y_{mt} = \sum_{i=1}^D \sum_{j=1}^{P_i} \beta_j^{[i]} x_{m(t-1)-m_i(j-1)}^{[i]} + \varepsilon_{mt}, \quad t = 1, \dots, T, \quad (1)$$

where for each variable  $i$ , we include  $P_i$  lags in the model with parameter  $\beta_j^{[i]}$  at lag  $j$ . The variables are assumed to be mean-centered such that no intercept is included and  $\varepsilon_{mt}$  denotes an error term. The total number of parameters to estimate is  $N := \sum_{i=1}^D P_i$ . Model (1) includes both standard autoregressive and mixed-frequency regressions, as illustrated in Examples 1 and 2.

**Example 1** (AR Models). The autoregressive model of order  $P$ ,  $\text{AR}(P)$ , given by

$$y_t = \sum_{j=1}^P \beta_j y_{t-j} + \varepsilon_t, \quad t = 1, \dots, T, \quad (2)$$

is a special case of Model (1), obtained by setting  $D = 1, m = m_1 = 1$  and denoting  $P = P_1, y_t = x_t^{[1]}$ . In this paper, we focus on modeling high-order autoregressive processes. In such settings, the dimensionality of the model increases with  $P$ , as adequately capturing the underlying dynamics may require the inclusion of many lags.

**Example 2** (Mixed-Frequency Models). Model (1) also accommodates unrestricted MIDAS regressions (Forni et al., 2015). For simplicity, consider the unrestricted MIDAS model

$$y_{mt} = \sum_{j=1}^{P_1} \beta_j^{[1]} x_{m(t-1)-(j-1)}^{[1]} + \sum_{j=1}^{P_2} \beta_j^{[2]} y_{m(t-1)-m(j-1)} + \varepsilon_{mt}, \quad t = 1, \dots, T, \quad (3)$$

with low-frequency response, single high-frequency explanatory variable  $x_t = x_t^{[1]}$  with  $P_1$  lags and  $P_2$  lags of the response ( $y_t = x_t^{[2]}$ ). A typical MIDAS set-up would consider a quarterly-monthly arrangement with  $m = 3$ . While equation (3) permits forecasting, nowcasting can be achieved by including the high-frequency explanatory variable at lags  $x_{mt-(j-1)}$  rather than  $x_{m(t-1)-(j-1)}$ .<sup>1</sup>

Model (3) can easily be extended to multiple explanatory variables with their own sampling frequency and lag structure. We focus on modeling mixed-frequency regressions where the curse of dimensionality arises due to two sources. First, the number of variables  $D$  may become large relative to the sample size  $T$ . Secondly, and specific to mixed-frequency models, we allow for the inclusion of high-frequency explanatory variables where the difference in sampling frequencies between the highest- and lowest-frequency ones can become substantial. In Section 6.2, for example, we model GDP growth using daily, weekly, monthly and quarterly variables, the frequency mismatches then range from  $m = 60$  (assuming 60 trading days in a quarter) over 20 (for day/month) to 5 (for day/week). Such large frequency mismatches further increase the dimensionality of the model, since the higher frequency variables typically require including more lags.

Examples 1 and 2 illustrate that the key drivers of the dimensionality in model (1) are the number of explanatory variables ( $D$ ), the number of lags ( $P_i$ s), and the frequency mismatches ( $m, m_i$ s). We address this curse of dimensionality by resorting to penalized estimation. A typical choice would consist of inducing sparsity, for instance via the Lasso (Tibshirani, 1996). Yet, in many practical applications with mixed-frequency time series, the lagged values are often highly correlated, but this is typically not handled well by the Lasso (e.g., Chapter 4 in Hastie et al., 2015). Moreover, it is likely that no single past observation affects the present but rather longer-run patterns, such as sums (or averages) across lags as in the Heterogeneous AutoRegressive (HAR) model of Corsi (2009). We therefore address the curse of dimensionality in model (1) through temporal lag aggregation (in addition to sparsity). Our penalized estimation routine determines in a data-driven way how to aggregate over past observations in a longer period. The dimensionality in model (1) is then reduced since many parameters will be estimated identically. We do not impose aggregation structures on the lags a priori. Instead, we employ temporal trees to guide the aggregation in a natural, data-driven way, as discussed in the following section.

---

<sup>1</sup>Model (3) uses notation that differs from the standard mixed-frequency literature; this is done for convenience and to facilitate the use of temporal aggregation in our modeling setup.

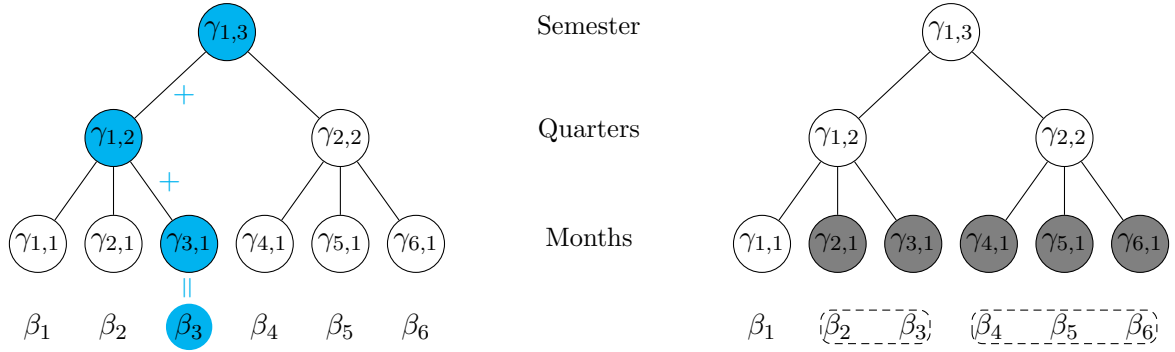


Figure 2: Toy example of a temporal tree aggregating months into quarters and a semester. Left panel: Re-parametrization of the original parameters  $\beta_j$  in terms of the  $\gamma$ s. The path from leaf 3 to the root, highlighted in blue, presents the re-parametrization of its corresponding coefficient:  $\beta_3 = \gamma_{3,1} + \gamma_{1,2} + \gamma_{1,3}$ . Similarly, the other descendants of  $\gamma_{1,2}$  are expressed with  $\beta_i = \gamma_{i,1} + \gamma_{1,2} + \gamma_{1,3}$  for  $i = 1, 2, 3$ , while the descendants of  $\gamma_{2,2}$  are  $\beta_j = \gamma_{j,1} + \gamma_{2,2} + \gamma_{1,3}$  for  $j = 4, 5, 6$ . Right panel: Effect of penalization where the nodes in gray are zeroed out, thereby giving  $\beta_1 = \gamma_{1,1} + \gamma_{1,2} + \gamma_{1,3}$ ,  $\beta_i = \gamma_{1,2} + \gamma_{1,3}$  for  $i = 2, 3$  and  $\beta_j = \gamma_{2,2} + \gamma_{1,3}$  for  $j = 4, 5, 6$ .

## 2.2 Temporal Aggregation with Trees

In Section 2.2.1, we first introduce temporal aggregation for autoregressive models, as in equation (2), using a single temporal tree. In Section 2.2.2, we discuss how the idea of temporal aggregation can be extended for the general mixed-frequency model (1) with multiple temporal trees.

### 2.2.1 A Temporal Tree for AutoRegressive Models

Consider autoregressive processes where the data are observed at high frequency (for instance daily). It is not always suitable to include each lag individually at that finest scale in Model (2), as high-frequency measurements can be noisy. Capturing effects at lower temporal resolutions may help reduce noise and amplify the underlying signal by revealing longer-run patterns. We leverage a temporal tree as side information to guide such temporal aggregation.

**Temporal Tree.** To guide lag aggregation in autoregressive model (2), we rely on a temporal tree. Time series naturally lend themselves to a tree structure, since finer time units can be grouped into coarser ones: Seconds form minutes, minutes form hours, hours form days, and so on. While our focus is on AR processes observed at relatively high sampling frequency, we illustrate the main idea of temporal aggregation using a smaller-scale toy example to keep the visualizations across this section concise. In particular, consider an AR process where data are observed monthly. Figure 2 displays a temporal tree where monthly lags (six leaves at the bottom) are aggregated naturally into two quarterly lags (internal nodes) and then into a single semester lag (root node). Moving up the tree thus corresponds to a natural transition from higher- to lower-frequency observations.

While the tree structure provides an intuitive way to perform temporal aggregation, in practice, the most suitable temporal aggregation level for the lags in model (2) is often unknown a priori. In our toy example, lags may be incorporated at monthly, quarterly, semiannual frequencies, or even a combination thereof. Our objective is therefore to allow the data to determine the appropriate temporal resolution at which lags should enter the model. To this end, we employ a reparametrization strategy on the parameters  $\beta_j$  of model (2), extending the approach of Yan and Bien (2021) to our time series setting. The temporal tree is hereby central to help identify, in a data-driven way, an appropriate temporal frequency at which lags should be included in model (2).

**Tree-Based Model Parameterization.** Let  $\mathcal{T}$  denote the tree that encodes the temporal aggregation structure across  $L$  different frequency levels. At each level  $l$ , there are  $p_l$  nodes, with  $p_1$  denoting the number of leaves at the bottom level and  $p_L = 1$  (the single root node). At each level  $l \in \{1, \dots, L-1\}$ , the  $p_l$  nodes are grouped into  $p_{l+1}$  parent nodes. Each parent node aggregates a fixed number  $K_l$  of consecutive child nodes, so that  $p_{l+1} = p_l/K_l$ . This defines the branching structure of the tree, with each group at level  $l$  aggregating  $K_l$  nodes from the previous level.

To illustrate this, we revisit the toy example in Figure 2. The tree has  $L = 3$  levels. The bottom level consists of  $p_1 = 6$  nodes, corresponding to the monthly lags. Those are grouped in triplets ( $K_1 = 3$ ) leading to the  $p_2 = 2$  quarterly nodes on level 2. The internal nodes are, in turn, grouped into a single node ( $K_2 = 2$ ), the root, representing a full semester of monthly observations.

The tree can now be used to naturally guide temporal aggregation of the lags in the AR model. We hereby aim to encourage aggregation of lags within a branch to form new, lower-frequency lags. To implement such tree-guided aggregation, we associate a coefficient  $\beta_j$  with every leaf of the tree ( $p_1 = P$  by construction) and encourage fusion of lags within a branch so that the descendant lags of that branch are aggregated when their effects are similar.

To enable fusion, each node in the tree (leaf, internal and root) gets assigned a new auxiliary parameter, denoted  $\gamma_{k,l}$ , where  $k = 1, \dots, p_l$  indexes the nodes on level  $l = 1, \dots, L$ . We then represent each original  $\beta$  parameter as the sum of the  $\gamma$  parameters along the path from its corresponding leaf to the root. The relation between the  $\beta_j$  and  $\gamma$ s can be expressed as

$$\beta_j = \sum_{l=1}^L \gamma_{\theta_{\mathcal{T}}(j,l)},$$

where the mapping function  $\theta : (\mathcal{T}, j, l) \rightarrow \theta_{\mathcal{T}}(j, l) := (k, l)$  uses the tree structure  $\mathcal{T}$ , the position of leaf  $j$ , and the level  $l$  to uniquely identify each node in the tree. The left panel of Figure 2

highlights such a path in blue, namely for parameter  $\beta_3$  corresponding to leaf  $j = 3$ . We then have  $\beta_3 = \gamma_{3,1} + \gamma_{1,2} + \gamma_{1,3}$ , using that at level 1,  $\theta_{\mathcal{T}(3,1)} = (3, 1)$ , at level 2,  $\theta_{\mathcal{T}(3,2)} = (1, 2)$ , and at level 3,  $\theta_{\mathcal{T}(3,3)} = (1, 3)$ .

Finally, stacking all  $N$  parameters in  $\beta$  (for the AR model  $N = P$ ) in a vector, we can write  $\beta = \mathbf{A}\gamma$ , where  $\mathbf{A} \in \{0, 1\}^{N \times |\mathcal{T}|}$  encodes the tree structure and the vector  $\gamma \in \mathbb{R}^{|\mathcal{T}| \times 1}$  is constructed by stacking the parameters from each level of the tree sequentially, starting with all level-1 (leaf) nodes ordered from left to right, followed by the level-2 nodes in the same order, and proceeding upward until the root node at level  $L$ . The entries of  $\mathbf{A}$  are given by

$$a_{j,p} = \begin{cases} 1 & \text{if the node at position } p \text{ lies on the path from } \gamma_{j,1} \text{ to } \gamma_{1,L}, \\ 0 & \text{otherwise.} \end{cases}$$

**Temporal Aggregation Through Penalization.** We reparametrize the  $\beta_j$ s in terms of the  $\gamma$ s since temporal aggregation can now be achieved by zeroing out  $\gamma$ s. Indeed, each branch in the tree reflects the aggregation of its descendant leaves. Zeroing out all  $\gamma$ s for all descendants of a particular branch in the tree, fuses the coefficients in this branch, leading to temporal aggregation.

In the toy example, zeroing out all monthly leaf nodes would result in the inclusion of its corresponding quarterly effect. In the right panel of Figure 2, we illustrate the effect of zeroing out  $\gamma$ s (their nodes are grayed out). For example, months 4 to 6 are no longer included individually in the model. Instead, their coefficients are equal ( $\beta_4 = \beta_5 = \beta_6 = \gamma_{2,2} + \gamma_{1,3}$ ), so that their aggregate quarterly effect is captured in the model.

By allowing each  $\gamma$  in the tree to be set to zero, we allow the model to flexibly determine the appropriate level of aggregation for each part of the lag space. In the same figure, the first three monthly lags display distinct behavior either remaining separate, hence not fused, in the model like the first monthly lag  $\beta_1$  or entering partially fused like the second and third monthly lags ( $\beta_2 = \beta_3 = \gamma_{1,2} + \gamma_{1,3}$ ). As a result, we can reduce the dimensionality of the AR model (2) by fusing certain lags, hence performing temporal aggregation, while still allowing for meaningful differences in the temporal dynamics when economically relevant and supported by the data.

*Remark 1.* Multiple configurations of the zeroed out auxiliary parameters  $\gamma$  may induce the same aggregation in the target parameter  $\beta$ . For instance, in the toy example, zeroing out  $\gamma_{2,2}$  in addition to the other zeroed out  $\gamma$ s leads to the same fusion as before (with this time  $\beta_j = \gamma_{1,3}$  for  $j = 4, 5, 6$ ). The non-uniqueness in terms of the  $\gamma$ s is not problematic, since the  $\beta$ s are the parameters of interest. Moreover, from a computational perspective, this non-uniqueness does not hinder estimation: The

optimization problem, introduced in Section 3, is convex in  $\beta$  and  $\gamma$  and they can be estimated in a computationally efficient way.

**Example 3 (HAR Model).** The Heterogeneous AutoRegressive (HAR) model by Corsi (2009) can be recovered through our temporal aggregation framework. Consider AR model (2) with  $P = 20$  daily lags. The temporal tree in Figure 3 encourages aggregation of the daily lags (20 leaves) into four weekly lags (internal nodes) and finally one single monthly lag (root). The sparsity structure on the  $\gamma$ s indicated in Figure 3 induces the following fusion constraints, namely  $\beta_1 = \gamma_{1,1} + \gamma_{1,2} + \gamma_{1,3}$ ,  $\beta_i = \gamma_{1,2} + \gamma_{1,3}$  for  $i = 2, \dots, 5$  and  $\beta_j = \gamma_{1,3}$  for  $j = 6, \dots, 20$ . Incorporating these constraints on the parameters of the AR(20) leads to the HAR model, namely

$$\begin{aligned} y_t &= \sum_{j=1}^{20} \beta_j y_{t-j} + \varepsilon_t \\ &= (\gamma_{1,1} + \gamma_{1,2} + \gamma_{1,3}) y_{t-1} + (\gamma_{1,2} + \gamma_{1,3}) \sum_{j=2}^5 y_{t-j} + \gamma_{1,3} \sum_{j=6}^{20} y_{t-j} + \varepsilon_t \\ &= \gamma_{1,1} y_{t-1} + \gamma_{1,2} \sum_{j=1}^5 y_{t-j} + \gamma_{1,3} \sum_{j=1}^{20} y_{t-j} + \varepsilon_t, \end{aligned}$$

where the second equality follows from substituting the sparsity constraints on  $\gamma$  depicted in Figure 3 and the third line rearranges terms to express the HAR model according to its daily ( $\beta^{(d)} = \gamma_{1,1}$ ), weekly ( $\beta^{(w)} = 5\gamma_{1,2}$ ), and monthly ( $\beta^{(m)} = 20\gamma_{1,3}$ ) effects.

Unlike the HAR model, we do not impose the aggregation structure a priori. Instead, the temporal tree serves only as guidance for potential temporal aggregations. The latter are determined in a data-driven manner through penalized estimation. In Section 3, we propose a penalized estimation procedure that leverages the tree as side information to guide temporal aggregation. In particular, the addition of an  $\ell_1$  penalty on the  $\gamma$  parameters in the objective function enables data-driven identification of a suitable temporal aggregation structure for the problem at hand.

### 2.2.2 Temporal Trees for Mixed-Frequency Models

The idea of temporal aggregation introduced in Section 2.2.1 for AR models can easily be extended to the general mixed-frequency model (1). We then assign a separate temporal tree for each explanatory variable. Specifically, for each variable  $i$ , a tree  $\mathcal{T}^{[i]}$  is constructed to govern the temporal aggregation of the lags associated with that variable. The leaves represent the highest recorded frequency for that variable whereas the root node represents the lowest temporal frequency of interest. Each variable  $i$  has its auxiliary parameter vector  $\gamma^{[i]}$  and matrix  $\mathbf{A}^{[i]}$  that relates the

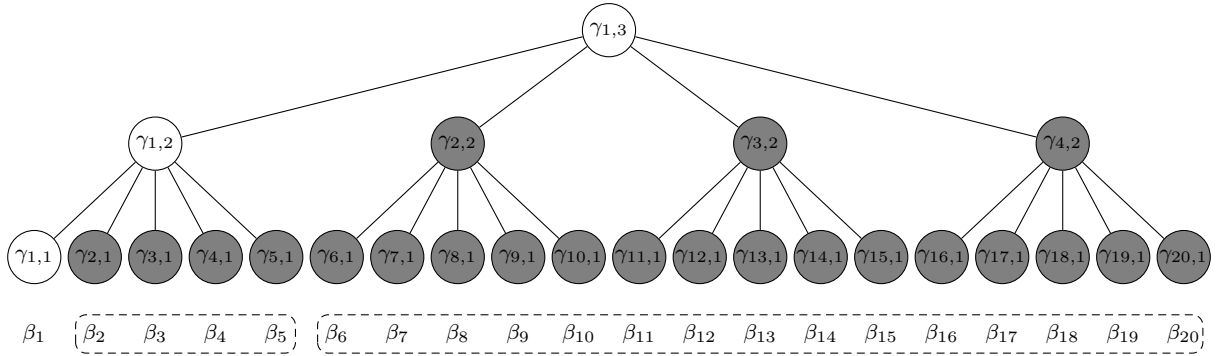


Figure 3: Temporal tree aggregating 20 days into four weeks and one month. The sparsity pattern on the  $\gamma$ s, where gray nodes are zeroed out, leads to recovery of the HAR model.

parameters  $\beta_j^{[2]}$  to the  $\gamma^{[i]}$ . The vector  $\boldsymbol{\gamma}$  is formed by stacking the individual vectors  $\boldsymbol{\gamma}^{[i]}$  vertically, ordered from variable 1 to  $D$ . Similarly, the matrix  $\mathbf{A}$  is constructed by placing the individual matrices  $\mathbf{A}^{[i]}$  on its diagonal, so that  $\mathbf{A} \in \{0, 1\}^{N \times M}$ , with  $M = \sum_{i=1}^D |\mathcal{T}^{[i]}|$ . Aggregation and fusion for variable  $i$  are performed within the tree corresponding to that variable, independently of all other variables. The resulting temporal aggregation for one variable does not affect the resulting temporal aggregation for another variable, enabling full flexibility.

**Example 4** (Mixed-Frequency Regressions with Multiple Trees). Consider mixed-frequency model (3) with a quarterly response and monthly explanatory variable (hence  $m = 3$ ). When including  $P_1 = 12$  monthly lags and  $P_2 = 4$  quarterly lags, the model takes the form

$$y_{3t} = \sum_{j=1}^{12} \beta_j^{[1]} x_{3(t-1)-(j-1)}^{[1]} + \sum_{j=1}^4 \beta_j^{[2]} y_{3(t-1)-3j} + \varepsilon_{3t}, \quad t = 1, \dots, T.$$

Figure 4 displays the temporal trees used for the monthly variable (in panel a) and the quarterly variable (in panel b), each aggregating to a yearly frequency at the root. The relationship between the  $N = 16$ -dimensional  $\boldsymbol{\beta}$ -vector and the  $M = 22$ -dimensional  $\boldsymbol{\gamma}$ -vector is given by

$$\boldsymbol{\beta} = \begin{bmatrix} \boldsymbol{\beta}^{[1]} \\ \boldsymbol{\beta}^{[2]} \end{bmatrix} = \begin{bmatrix} \mathbf{A}^{[1]} & \mathbf{O}_{12 \times 5} \\ \mathbf{O}_{4 \times 17} & \mathbf{A}^{[2]} \end{bmatrix} \begin{bmatrix} \boldsymbol{\gamma}^{[1]} \\ \boldsymbol{\gamma}^{[2]} \end{bmatrix} = \mathbf{A} \boldsymbol{\gamma},$$

where  $\boldsymbol{\beta}^{[1]} \in \mathbb{R}^{12 \times 1}$  collects the monthly and  $\boldsymbol{\beta}^{[2]} \in \mathbb{R}^{4 \times 1}$  the quarterly parameters,  $\boldsymbol{\gamma}^{[1]} \in \mathbb{R}^{17 \times 1}$  the auxiliary monthly and  $\boldsymbol{\gamma}^{[2]} \in \mathbb{R}^{5 \times 1}$  the auxiliary quarterly parameters,  $\mathbf{A}^{[1]} \in \{0, 1\}^{12 \times 17}$  and  $\mathbf{A}^{[2]} \in \{0, 1\}^{4 \times 5}$ ,  $\mathbf{A} \in \{0, 1\}^{16 \times 22}$  and  $\mathbf{O}$  is a conformable matrix of zeros.

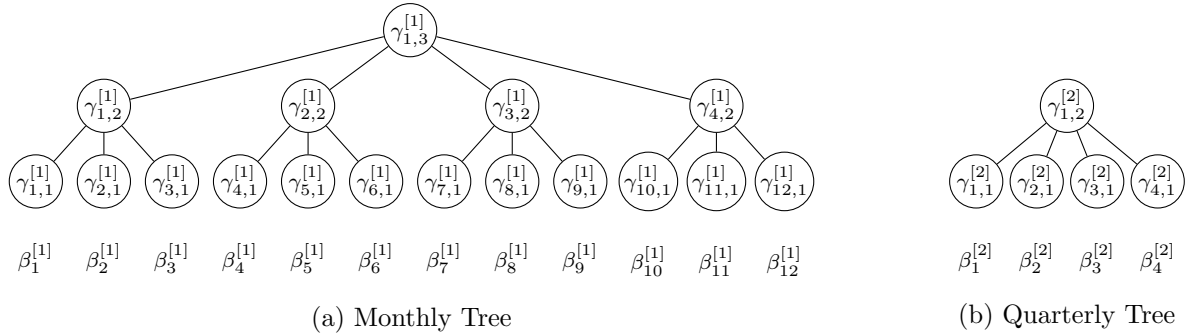


Figure 4: Tree structures for a mixed-frequency regression with a quarterly response and monthly explanatory variable.

### 3 Sparse Tree-Based Aggregation through Penalized Estimation

In Section 3.1, we introduce our penalized estimation procedure. Details on our algorithmic implementation and the hyperparameter tuning are discussed in Sections 3.2 and 3.3 respectively.

#### 3.1 Estimator

First, consider model (1) in compact matrix form  $\mathbf{y} = \mathbf{X}\boldsymbol{\beta} + \boldsymbol{\varepsilon}$ , where  $\mathbf{y} \in \mathbb{R}^{T \times 1}$  is the response vector,  $\mathbf{X} \in \mathbb{R}^{T \times N}$  is the matrix of explanatory variables, containing the lags of  $x_t^{[i]}$  in its columns for  $i = 1, \dots, D$ ,  $\boldsymbol{\beta} \in \mathbb{R}^{N \times 1}$  is the parameter vector, and  $\boldsymbol{\varepsilon} \in \mathbb{R}^{T \times 1}$  contains the errors.

To estimate the model parameters, we propose the *Sparse Tree-Aggregation for Time Series Regressions (StarTime)* estimator, which is defined as the solution to the following objective

$$\tilde{\boldsymbol{\beta}}_{\lambda_1, \lambda_2}, \tilde{\boldsymbol{\gamma}}_{\lambda_1, \lambda_2} = \arg \min_{\boldsymbol{\beta}, \boldsymbol{\gamma}} \left\{ \frac{1}{2T} \|\mathbf{y} - \mathbf{X}\boldsymbol{\beta}\|_2^2 + \lambda_1 \|\boldsymbol{\gamma}\|_1 + \lambda_2 \|\boldsymbol{\beta}\|_1 \text{ s.t. } \boldsymbol{\beta} = \mathbf{A}\boldsymbol{\gamma} \right\}, \quad (4)$$

where the first part in the objective is the usual sum of squared residuals, the second part consists of the penalty terms on  $\boldsymbol{\gamma}$  and  $\boldsymbol{\beta}$ , and the constraint  $\boldsymbol{\beta} = \mathbf{A}\boldsymbol{\gamma}$  imposes the tree correspondence between the  $\boldsymbol{\gamma}$ 's and  $\boldsymbol{\beta}$ 's, as explained in Section 2.2. The penalty  $\lambda_1 \|\boldsymbol{\gamma}\|_1$  induces sparsity on the tree nodes, encouraging temporal aggregation of the lags where appropriate. The  $\lambda_2 \|\boldsymbol{\beta}\|_1$  encourages direct sparsity on the lagged coefficients. The tuning parameter  $\lambda_1$  controls the level of aggregation: Larger values of  $\lambda_1$  result in a higher degree of aggregation, whereas  $\lambda_2$  controls the degree of sparsity. StarTime can thus perform joint estimation, temporal aggregation and lag selection. When  $\lambda_1 = 0$ , StarTime reduces to the classical Lasso estimator.

In addition to the StarTime estimator defined in equation (4), referred to as Simple StarTime in the remainder, we also consider a ‘post-selection’ variant. We refer to this variant as ‘Post StarTime’. Given the sparsity and aggregation pattern in  $\tilde{\boldsymbol{\beta}}$ , we refit the model using OLS on the

reduced set of selected and potentially temporally aggregated variables. This two-stage procedure can improve estimation accuracy by removing the bias induced by the penalties.

Formally, let  $\tilde{\boldsymbol{\beta}} \in \mathbb{R}^{N \times 1}$  denote the vector encoding the selected and aggregated variables. Denote the vector collecting the unique, non-zero entries of  $\tilde{\boldsymbol{\beta}}$  by  $\tilde{\boldsymbol{\phi}} \in \mathbb{R}^{Q \times 1}$ , where  $Q$  denotes the number of unique, non-zero values in  $\tilde{\boldsymbol{\beta}}$ . The aggregation matrix  $\tilde{\mathbf{W}} \in \mathbb{R}^{N \times Q}$  is given by

$$\tilde{w}_{j,\ell} = \begin{cases} 1 & \text{if } \tilde{\beta}_j = \tilde{\phi}_\ell \\ 0 & \text{otherwise} \end{cases} \quad \text{for } j = 1, \dots, N, \ell = 1, \dots, Q.$$

We can then write  $\tilde{\boldsymbol{\beta}} = \tilde{\mathbf{W}}\tilde{\boldsymbol{\phi}}$  and  $\mathbf{X}\tilde{\boldsymbol{\beta}} = \mathbf{X}\tilde{\mathbf{W}}\tilde{\boldsymbol{\phi}}$ . The corresponding aggregated matrix is  $\tilde{\mathbf{X}} = \mathbf{X}\tilde{\mathbf{W}}$ , where the  $\ell$ -th column of  $\tilde{\mathbf{X}}$  is the sum of the columns of  $\mathbf{X}$  corresponding to indices  $j$  for which  $\tilde{\beta}_j = \tilde{\phi}_\ell$ , and columns with  $\tilde{\beta}_j = 0$  are omitted. We then perform OLS estimation with  $\mathbf{y}$  as response and  $\tilde{\mathbf{X}}$  as design matrix to obtain  $\hat{\boldsymbol{\phi}} = (\tilde{\mathbf{X}}^\top \tilde{\mathbf{X}})^{-1} \tilde{\mathbf{X}}^\top \mathbf{y}$ . The last step consists of mapping the obtained  $\hat{\boldsymbol{\phi}}$  onto  $\hat{\boldsymbol{\beta}} \in \mathbb{R}^{N \times 1}$ , to obtain the Post StarTime estimator  $\hat{\boldsymbol{\beta}} = \tilde{\mathbf{W}}\hat{\boldsymbol{\phi}}$ .

### 3.2 Algorithm

To solve (4), we develop an alternating direction method of multipliers (ADMM) algorithm (Boyd et al., 2011), used to decompose complex convex optimization problems into simpler subproblems. Our ADMM algorithm is based on solving the equivalent formulation of (4)

$$\begin{aligned} \min_{\substack{\boldsymbol{\beta}^{(1)}, \boldsymbol{\beta}^{(2)}, \boldsymbol{\beta}^{(3)}, \boldsymbol{\beta} \\ \boldsymbol{\gamma}^{(1)}, \boldsymbol{\gamma}^{(2)}, \boldsymbol{\gamma}}} & \left\{ \frac{1}{2T} \|\mathbf{y} - \mathbf{X}\boldsymbol{\beta}^{(1)}\|_2^2 + \lambda_1 \|\boldsymbol{\gamma}^{(1)}\|_1 + \lambda_2 \|\boldsymbol{\beta}^{(2)}\|_1 \right. \\ \text{s.t. } & \left. \boldsymbol{\beta}^{(3)} = \mathbf{A}\boldsymbol{\gamma}^{(2)}, \boldsymbol{\beta} = \boldsymbol{\beta}^{(1)} = \boldsymbol{\beta}^{(2)} = \boldsymbol{\beta}^{(3)}, \boldsymbol{\gamma} = \boldsymbol{\gamma}^{(1)} = \boldsymbol{\gamma}^{(2)} \right\}, \end{aligned} \quad (5)$$

where additional copies of  $\boldsymbol{\beta}$  (namely  $\boldsymbol{\beta}^{(1)}, \boldsymbol{\beta}^{(2)}, \boldsymbol{\beta}^{(3)}$ ) and  $\boldsymbol{\gamma}$  (namely  $\boldsymbol{\gamma}^{(1)}, \boldsymbol{\gamma}^{(2)}$ ) are introduced to efficiently decouple the optimization problem, whereas the global  $\boldsymbol{\beta}$  and  $\boldsymbol{\gamma}$  ensure the different subproblems are in agreement. The subproblems of our ADMM routine are identical to the subproblems of Yan and Bien (2021); their Appendix D.1 contains full details.

Regarding convergence of the ADMM algorithm, we evaluate the maximum absolute change between the estimated  $\boldsymbol{\beta}$  at iterations  $i$  and  $i + 1$  and terminate the ADMM procedure when this difference falls below a threshold of  $10^{-5}$ . Furthermore, throughout the paper, we fix the maximum number of iterations at 1000 and set the ADMM penalty parameter to  $\rho = 1$ .

### 3.3 Tuning Parameters

We select the tuning parameters  $\lambda_1$  and  $\lambda_2$  by using grid search combined with a Bayesian Information Criterion (BIC). First, we construct a  $10 \times 10$  grid of candidate  $(\lambda_1, \lambda_2)$  values. For each pair on the grid, we estimate the model and compute the following information criterion

$$\text{BIC}_{\lambda_1, \lambda_2} = \tilde{T} \ln \left( \frac{\hat{\sigma}_{\lambda_1, \lambda_2}^2}{\tilde{T}} \right) + Q_{\lambda_1, \lambda_2} \ln(\tilde{T}) + \infty \mathbb{1} \left\{ \frac{Q_{\lambda_1, \lambda_2}}{\tilde{T}} > c \right\}, \quad (6)$$

where  $\hat{\sigma}_{\lambda_1, \lambda_2}^2 = \|\mathbf{y} - \mathbf{X}\hat{\boldsymbol{\beta}}\|_2^2$ , with  $\hat{\boldsymbol{\beta}}$  the Post StarTime estimate,  $\tilde{T} = T - P_{\max}$  is the effective sample size with  $P_{\max}$  the number of lags we maximally lose, and  $Q_{\lambda_1, \lambda_2}$  is the effective number of parameters, that is, the number of unique, non-zero components of  $\hat{\boldsymbol{\beta}}$  for a given  $(\lambda_1, \lambda_2)$  pair. The inclusion of the extra complexity penalty on  $Q_{\lambda_1, \lambda_2}/\tilde{T}$  helps prevent the model from selecting pairs that would result in the inclusion of too many parameters, which could lead to overfitting. If the ratio exceeds the threshold,  $c \in [0, 1]$ , we add a large penalty to the BIC, which prevents the algorithm from selecting that pair. The threshold value  $c$  can be adjusted based on user preference and the complexity of the problem. In high-dimensional settings, we advise using a lower threshold to better control model complexity. In the low-dimensional settings, the threshold can be set at one, so that the usual BIC applies and no extra penalty is used. The intuition for this approach is similar to that of [Chen and Chen \(2012\)](#), in which the authors introduce the EBIC, which also contains an extra penalty for model complexity in case  $N \geq \tilde{T}$ . After evaluating the model for all 100 combinations of  $(\lambda_1, \lambda_2)$  on the grid, we select the pair that yields the lowest BIC value.

Finally, to construct the  $\lambda$ -grid, we first determine maximum values such that respectively all  $\hat{\boldsymbol{\gamma}}$  and  $\hat{\boldsymbol{\beta}}$  coefficients become zero. We take  $\lambda_1^{\max} = \max |(\mathbf{X}\mathbf{A})^\top \mathbf{y}|/\tilde{T}$  and  $\lambda_2^{\max} = \max |\mathbf{X}^\top \mathbf{y}|/\tilde{T}$ . The minimum value is set as a fixed fraction of this maximum, with the fraction depending on the dimensions of the data: If  $\tilde{T} > N$ , then we set  $\lambda_i^{\min} = \lambda_i^{\max} \times 10^{-4}$  and if  $N \geq \tilde{T}$ , then  $\lambda_i^{\min} = \lambda_i^{\max} \times 10^{-7}$  (for  $i = 1, 2$ ) to cover a broader range in case of high dimensionality. The sequence of  $\lambda$  values is then spaced evenly on a logarithmic scale between these endpoints.

## 4 Theoretical Properties

We derive an error bound for StarTime (Theorem 1) which is then used to establish prediction and estimation consistency, allowing for the number of parameters to grow faster than the sample size (Corollary 1). We adopt the general framework of Chapter 6 in [Bühlmann and van de Geer \(2011\)](#). We first introduce the high-level assumptions underlying our analysis, and then present the main

results. All auxiliary lemmas and proofs are collected in Appendix A.1 and A.2 respectively.

We use the following notation. For any vector  $\mathbf{u} \in \mathbb{R}^N$  and  $r \geq 1$ , the  $\ell_r$ -norm is defined as  $\|\mathbf{u}\|_r = \left(\sum_{i=1}^N |u_i|^r\right)^{1/r}$ . For  $r = 0$ , we use the convention  $\|\mathbf{u}\|_0 = \sum_{i=1}^N \mathbb{I}(u_i \neq 0)$ , with  $\mathbb{I}(\cdot)$  the indicator function. The  $\ell_\infty$ -norm is defined as  $\|\mathbf{u}\|_\infty = \max_i |u_i|$  for vectors, and element-wise as  $\|\mathbf{A}\|_\infty = \max_{i,j} |A_{i,j}|$  for matrices. In this section and accompanying proofs,  $C$  denotes a generic positive finite constant. Its value may change from line to line, absorbing other constants to streamline exposition, but it is always independent of time and the cross-sectional dimension.

We consider the linear model in matrix notation  $\mathbf{y} = \mathbf{X}\boldsymbol{\beta}^0 + \boldsymbol{\varepsilon}$ ,

where  $\mathbf{y} \in \mathbb{R}^{T \times 1}$ ,  $\mathbf{X} \in \mathbb{R}^{T \times N}$ ,  $\boldsymbol{\varepsilon} \in \mathbb{R}^{T \times 1}$  and  $\boldsymbol{\beta}^0 \in \mathbb{R}^{N \times 1}$  denotes the true parameter value. Since our analysis concerns dependent processes, we adopt a general time series framework in which both the regressors  $\mathbf{x}_t$  (denoting the  $t$ -th row of  $\mathbf{X}$ ) and the errors  $\varepsilon_t$  are permitted to be non-Gaussian, serially correlated and heteroskedastic. To accommodate this, we adopt the following assumption on  $\mathbf{z}_t := (\mathbf{x}_t^\top, \varepsilon_t)^\top$  which corresponds to Assumption 1 in Adamek et al. (2023).

**Assumption 1** (Assumption 1 in Adamek et al., 2023). *Let  $\mathbf{z}_t = (\mathbf{x}_t^\top, \varepsilon_t)^\top$ , and let there exist some constants  $\bar{m} > \tilde{m} > 2$ , and  $d \geq \max\{1, (\bar{m}/\tilde{m} - 1)/(\bar{m} - 2)\}$  such that*

(i) *Let  $\mathbb{E}[\mathbf{z}_t] = \mathbf{0}$ ,  $\mathbb{E}[\mathbf{x}_t \varepsilon_t] = \mathbf{0}$ , and  $\max_{1 \leq j \leq N+1, 1 \leq t \leq T} \mathbb{E}|z_{j,t}|^{2\bar{m}} \leq C$ .*

(ii) *Let  $\mathbf{s}_{T,t}$  denote a  $k(T)$ -dimensional triangular array that is  $\alpha$ -mixing of size  $-d/(1/\tilde{m} - 1/\bar{m})$  with  $\sigma$ -field  $\mathcal{F}_t^s := \sigma\{\mathbf{s}_{T,t}, \mathbf{s}_{T,t-1}, \dots\}$  such that  $\mathbf{z}_t$  is  $\mathcal{F}_t^s$ -measurable. The process  $\{z_{j,t}\}$  is  $L_{2\bar{m}}$ -near-epoch-dependent (NED) of size  $-d$  on  $\mathbf{s}_{T,t}$  with positive bounded NED constants, uniformly over  $j = 1, \dots, N + 1$ .*

The near-epoch dependence (NED) framework in Assumption 1 encompasses a broad class of commonly encountered time series processes. These include, but are not limited to, linear processes including ARMA models, various stochastic volatility and GARCH specifications, and strong mixing processes. For further discussion and formal definitions, we refer the reader to Adamek et al. (2023).

To derive an error bound for StarTime in a high-dimensional time series set-up, we first rewrite the objective function such that the penalties are uniquely expressed in terms of  $\boldsymbol{\gamma}$ . We do this to streamline notation and since we can express the effective sparsity in terms of the non-zero elements of  $\boldsymbol{\gamma}^0$  (see Assumption 2).

Using  $\boldsymbol{\beta} = \mathbf{A}\boldsymbol{\gamma}$ , we define  $w(\boldsymbol{\gamma}) \in \mathbb{R}^{(N+M) \times 1}$  as given by

$$w(\boldsymbol{\gamma}) := \begin{pmatrix} \mathbf{A} \\ \mathbf{I}_M \end{pmatrix} \boldsymbol{\gamma} := \mathbf{D}\boldsymbol{\gamma}.$$

Additionally, we set  $\lambda_1 = \lambda_2 = \lambda$  to avoid notational clutter. This restriction can be relaxed at the cost of more cumbersome notation and exposition. The objective function is then given by

$$\begin{aligned} \frac{1}{2T} \|\mathbf{y} - \mathbf{X}\boldsymbol{\beta}\|_2^2 + \lambda_1 \|\boldsymbol{\gamma}\|_1 + \lambda_2 \|\boldsymbol{\beta}\|_1 &= \frac{1}{2T} \|\mathbf{y} - \mathbf{X}\boldsymbol{\beta}\|_2^2 + \lambda \|\boldsymbol{\gamma}\|_1 + \lambda \|\mathbf{A}\boldsymbol{\gamma}\|_1 \\ &= \frac{1}{2T} \|\mathbf{y} - \mathbf{X}\boldsymbol{\beta}\|_2^2 + \lambda \|w(\boldsymbol{\gamma})\|_1. \end{aligned}$$

To apply StarTime successfully,  $\boldsymbol{\beta}^0$  must be ‘sparse’ with respect to our chosen penalty.

**Assumption 2** (Sparsity). *Assume the parameter vectors  $\boldsymbol{\beta}^0$  and  $\boldsymbol{\gamma}^0$  admit the representation*

$$\boldsymbol{\beta}^0 = \mathbf{W}\boldsymbol{\phi}^0 = \mathbf{A}\mathbf{S}\boldsymbol{\phi}^0 \quad \text{and} \quad \boldsymbol{\gamma}^0 = \mathbf{S}\boldsymbol{\phi}^0, \tag{7}$$

where  $\mathbf{W} \in \{0, 1\}^{N \times Q}$  is an aggregation matrix describing the coarsest aggregation structure of  $\boldsymbol{\beta}^0$ . We assume that this aggregation structure is contained in  $\mathbf{A}$ : There exists a column-selection matrix  $\mathbf{S} \in \mathbb{R}^{M \times Q}$ , with exactly one non-zero entry in each column, such that  $\mathbf{W} = \mathbf{A}\mathbf{S}$ . The parameter  $\boldsymbol{\gamma}^0$  is uniquely determined by  $\mathbf{S}$  and  $\boldsymbol{\phi}^0$ . We then define the active set on  $\boldsymbol{\gamma}^0$  as

$$S_0 := \left\{ l \in \{1, \dots, M\} : \gamma_l^0 \neq 0 \right\}, \quad s_0 := |S_0| = Q.$$

As discussed in Remark 1, multiple  $\boldsymbol{\gamma}$ ’s may induce the same aggregation in  $\boldsymbol{\beta}$ . Following Yan and Bien (2021), we therefore adopt their unique coarsest aggregating representation when uniquely defining  $\boldsymbol{\gamma}^0$  in terms of  $\mathbf{S}$  and  $\boldsymbol{\phi}^0$ . The effective sparsity in our error bound is  $s_0 = \|\boldsymbol{\gamma}^0\|_0$ . The parameter of interest  $\boldsymbol{\beta}^0$  inherits its aggregation structure from  $\boldsymbol{\gamma}^0$  and does not introduce additional free parameters.

In the remainder, let  $w(\boldsymbol{\gamma})_{S_0} := \mathbf{D}_{S_0}\boldsymbol{\gamma}_{S_0}$  denote the subvector restricted to the non-zero indices in  $\boldsymbol{\gamma}^0$ , where  $\mathbf{D}_{S_0}$  subsets the columns of  $\mathbf{D}$  in accordance. Let  $w(\boldsymbol{\gamma})_{S_0^c} := \mathbf{D}_{S_0^c}\boldsymbol{\gamma}_{S_0^c}$  denote the subvector restricted to the zero indices in  $\boldsymbol{\gamma}^0$ ; by construction  $w(\boldsymbol{\gamma}^0)_{S_0^c} = \mathbf{0}$ .

*Remark 2.* Sparsity in  $\boldsymbol{\gamma}^0$  encourages aggregation in  $\boldsymbol{\beta}^0$  by limiting the number of unique (non-zero) components in  $\boldsymbol{\beta}^0$ . While Assumption 2 only restricts the total number of non-zero components in

$\gamma^0$ , setting an internal node in the tree to zero produces effective aggregation in practice only if several of its descendants are also zero.

To obtain our desired bounds, we require a regularity condition on  $\mathbf{X}$  that rules out excessive collinearity in sparse directions. The estimation error can be restricted to vectors that satisfy the cone condition  $\|w(\boldsymbol{\gamma})_{S_0^c}\|_1 \leq 3 \|w(\boldsymbol{\gamma})_{S_0}\|_1$  (see Lemma 4 in Appendix A.1), so that deviations outside  $S_0$  are controlled by deviations on  $S_0$ . Let  $\boldsymbol{\Sigma} := \sum_{t=1}^T \mathbb{E}[\mathbf{x}_t \mathbf{x}_t^\top]/T$  denote the population covariance matrix of  $\mathbf{X}$ . The compatibility condition formalizes that, on this cone,  $\boldsymbol{\beta}^\top \boldsymbol{\Sigma} \boldsymbol{\beta}$  is sufficiently large relative to the  $\ell_1$ -norm of the coordinates on  $S_0$ .

**Assumption 3** (Compatibility Condition). *Assume the compatibility condition holds for the set  $S_0$ : There exists a  $\rho_\Sigma > 0$  such that for every  $\boldsymbol{\gamma}$  satisfying  $\|w(\boldsymbol{\gamma})_{S_0^c}\|_1 \leq 3 \|w(\boldsymbol{\gamma})_{S_0}\|_1$ ,*

$$\rho_\Sigma^2 \|w(\boldsymbol{\gamma})_{S_0}\|_1^2 \leq s_0 \boldsymbol{\beta}^\top \boldsymbol{\Sigma} \boldsymbol{\beta}. \quad (8)$$

This assumption is standard in Lasso theory and weaker than requiring the full Gram matrix to be well-conditioned; it only imposes control on  $\boldsymbol{\Sigma}$  along a restricted set of directions. We impose the compatibility condition on the population covariance rather than on the sample covariance  $\hat{\boldsymbol{\Sigma}} := \mathbf{X}^\top \mathbf{X}/T$ , because verifying conditions on the former is generally easier than doing so on the sample matrix (e.g., Medeiros and Mendes, 2016; Adamek et al., 2023). The proof then proceeds by showing that, under the conditions of Assumption 3,  $\hat{\boldsymbol{\Sigma}}$  is sufficiently close to  $\boldsymbol{\Sigma}$  with high probability, allowing the compatibility condition to carry over to the sample-based version.

While Assumption 3 addresses the deterministic part of the argument, we also need to control the stochastic term  $\|\mathbf{X}^\top \boldsymbol{\varepsilon}\|_\infty/T$ , which determines the choice of the tuning parameter  $\lambda$ . We therefore introduce a high-probability event under which choosing  $\lambda$  sufficiently large ensures that the penalty dominates the stochastic term. Define the set  $\mathcal{J} = \{\|\mathbf{X}^\top \boldsymbol{\varepsilon}\|_\infty/T \leq \lambda_0\}$  where  $\lambda_0 > 0$  is a bound for the empirical process. On  $\mathcal{J}$ , choosing  $\lambda \geq 2\lambda_0$  ensures that the penalty dominates the empirical process term in the basic inequality of Lemma 1 in Appendix A.1.

Lemma 2 provides a high-probability bound for the empirical process and thus for the event  $\mathcal{J}$ , which motivates the choice of  $\lambda$ . In addition, since Assumption 3 is imposed on the population covariance matrix  $\boldsymbol{\Sigma}$ , we introduce the event  $\mathcal{C}(S_0) := \{\|\hat{\boldsymbol{\Sigma}} - \boldsymbol{\Sigma}\|_\infty \leq C/s_0\}$ , under which Lemma 6 implies that the compatibility condition carries over to the sample Gram matrix  $\hat{\boldsymbol{\Sigma}}$  on the relevant cone. Conditional on  $\mathcal{J} \cap \mathcal{C}(S_0)$ , combining the basic inequality in Lemma 1, the cone restriction (Lemma 4) and sample compatibility then yields the bound in Theorem 1.

**Theorem 1.** *Suppose that Assumptions 1, 2, 3 hold for the active set  $S_0$  with constant  $\rho_0 > 0$ . Then, on the events  $\mathcal{J}$  and  $\mathcal{C}(S_0)$ , for  $\lambda \geq 2\lambda_0$ , we have:*

$$\frac{1}{2T} \left\| \mathbf{X}(\hat{\boldsymbol{\beta}} - \boldsymbol{\beta}^0) \right\|_2^2 + \lambda \|w(\hat{\boldsymbol{\gamma}} - \boldsymbol{\gamma}^0)\|_1 \leq \frac{8\lambda^2 s_0}{\rho_0^2}. \quad (9)$$

Setting  $\lambda := 2C \frac{N^{1/\tilde{m}} \ln(\ln(T))^{1/\tilde{m}}}{\sqrt{T}}$ , the bound in (9) holds with probability  $\mathbb{P}(\mathcal{J} \cap \mathcal{C}(S_0)) \geq 1 - C(\ln(\ln(T)))^{-1}$  for  $N, T$  sufficiently large.

**Corollary 1.** *Under Assumptions 1, 2 and 3, Theorem 1 gives the following bounds with probability at least  $\mathbb{P}(\mathcal{J} \cap \mathcal{C}) \geq 1 - C(\ln(\ln(T)))^{-1}$  for  $N, T$  large enough,*

$$(i) \quad \frac{1}{T} \left\| \mathbf{X}(\hat{\boldsymbol{\beta}} - \boldsymbol{\beta}^0) \right\|_2^2 \leq \frac{C\lambda^2 s_0}{\rho^2}$$

$$(ii) \quad \|w(\hat{\boldsymbol{\gamma}} - \boldsymbol{\gamma}^0)\|_1 \leq \frac{C\lambda s_0}{\rho_0^2}.$$

Corollary 1 follows directly from the oracle inequality in Theorem 1. On the event  $\mathcal{J} \cap \mathcal{C}(S_0)$ , the bound in (9) controls the sum of two non-negative terms. Consequently, each term is individually bounded by the same right-hand side. This yields the stated prediction and  $\ell_1$ -type error bounds with probability at least  $\mathbb{P}(\mathcal{J} \cap \mathcal{C}(S_0))$ .

## 5 Simulations

We assess the performance of the StarTime estimator against suitable benchmarks in autoregressive (Section 5.1) and mixed-frequency (Section 5.2) data generating processes (DGPs).

For each scheme, we evaluate the performance of the estimators on three performance metrics related to estimation accuracy, aggregation and sparsity recovery. Regarding estimation accuracy, we compute the *Mean Squared Error*:

$$\text{MSE} = \frac{1}{N} \sum_{i=1}^D \sum_{j=1}^{P_i} \left( \hat{\beta}_j^{[i]} - \beta_j^{[i]} \right)^2.$$

The lower the MSE, the better the accuracy. For aggregation recovery, we let each set of identical (zero or non-zero) components of  $\boldsymbol{\beta}$  form a group and compare this ‘true’ grouping structure to the estimated one based on  $\hat{\boldsymbol{\beta}}$  using the *Adjusted Rand Index* (Hubert and Arabie, 1985):

$$\text{ARI} = \frac{\sum_{ij} \binom{n_{ij}}{2} - \frac{\sum_i \binom{a_i}{2} \sum_j \binom{b_j}{2}}{\binom{N}{2}}}{\frac{1}{2} \left[ \sum_i \binom{a_i}{2} + \sum_j \binom{b_j}{2} \right] - \frac{\sum_i \binom{a_i}{2} \sum_j \binom{b_j}{2}}{\binom{N}{2}}},$$

where  $n_{ij}$  is the number of elements in both group  $i$  of  $\beta$  and group  $j$  of  $\hat{\beta}$ ,  $a_i$  and  $b_j$  are the totals for the  $i$ th true and  $j$ th estimated group, and  $N$  is the number of elements in  $\beta$ . The closer the ARI to one, the better the aggregation recovery.

For sparsity recovery, we compute the *F1 score*:

$$F1 = \frac{2 \cdot TP}{2 \cdot TP + FP + FN}, \quad (10)$$

where TP denotes the number of true positives (both  $\beta_j^{[i]}$  and  $\hat{\beta}_j^{[i]}$  are non-zero), FP the number of false positives ( $\hat{\beta}_j^{[i]}$  is non-zero,  $\beta_j^{[i]}$  is zero), and FN the number of false negatives ( $\hat{\beta}_j^{[i]}$  is zero,  $\beta_j^{[i]}$  is non-zero). The closer the F1 score to one, the better the sparsity recovery. We compute these metrics in each simulation run, and report results averaged across all simulation runs. Throughout the simulation study, we take 500 simulation runs. All simulations were conducted in R ([R Core Team, 2025](#)) using the `StarTime` package.

## 5.1 Autoregressive DGPs

### 5.1.1 Data Generating Processes

We consider three autoregressive DGPs, inspired by the HAR model.

**DGP 1** covers the case of aggregation but no sparsity:

$$y_t = 0.3y_{t-1} - 0.2 \sum_{j=2}^5 y_{t-j} + 0.02 \sum_{j=6}^{15} y_{t-j} + 0.01 \sum_{j=16}^{20} y_{t-j} + \varepsilon_t.$$

**DGP 2** covers the case of aggregation and sparsity:

$$y_t = 0.5y_{t-1} - 0.1 \sum_{j=2}^5 y_{t-j} + 0 \sum_{j=6}^{20} y_{t-j} + \varepsilon_t.$$

**DGP 3** covers the case of sparsity without aggregation:

$$y_t = 0.5y_{t-1} - 0.1y_{t-2} + 0.2y_{t-3} + 0.05y_{t-4} - 0.3y_{t-5} + 0 \sum_{j=6}^{20} + \varepsilon_t.$$

For all three cases, we take  $\varepsilon_t \sim \mathcal{N}(0, 1)$ ,  $T = 100$  and  $T = 200$  with a burn-in of 200 observations. As a general note, to facilitate comparisons of sparsity and aggregation structures across DGPs, we explicitly display covariates with zero coefficients in the model equations. Although these covariates do not contribute to the data-generating process, they are included during estimation.

### 5.1.2 Estimators

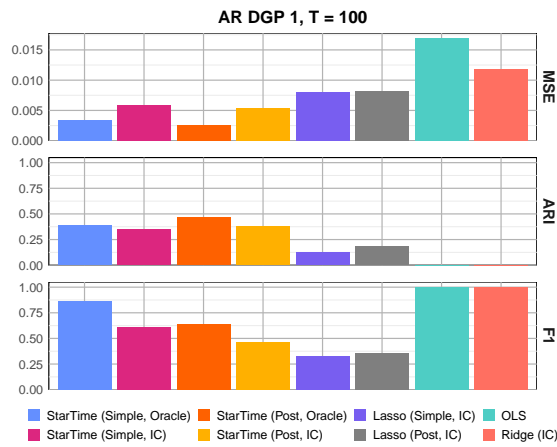
We compare StarTime to three benchmarks: *OLS*, *Lasso* (Tibshirani, 1996) and *Ridge* (Hoerl and Kennard, 1970). OLS serves as a baseline estimator without penalization. Lasso serves as a sparse benchmark that does not perform temporal aggregation. Lasso corresponds to StarTime with  $\lambda_1 = 0$ . For fair comparison, we compute the Lasso with the same ADMM algorithm as StarTime and also include a post-selection variant. The tuning parameter is selected using the BIC. Ridge serves as a regularized benchmark without sparsity or aggregation. We use the implementation in the `glmnet` package (Friedman et al., 2010). The tuning parameter is selected using the BIC.

For StarTime, we consider both Simple and Post StarTime (see Section 3.1) with a tree structure consisting of 20 (daily) leaves, aggregated into four (weekly) internal nodes and one final (monthly) root, as illustrated in Figure 2. While this tree structure is inspired by the HAR model, we do not impose its temporal aggregation constraints a priori. Instead, StarTime explores the lag space in a computationally efficient manner, imposing aggregation and sparsity constraints only when supported by the data. To select the tuning parameters, we use the BIC with  $c = 1$ . For Simple StarTime, we use  $\tilde{\beta}$  instead of  $\hat{\beta}$  when computing the BIC in (6). We also report ‘Oracle’ results for selected tuning parameters that minimize the MSE against which the BIC results can be compared.

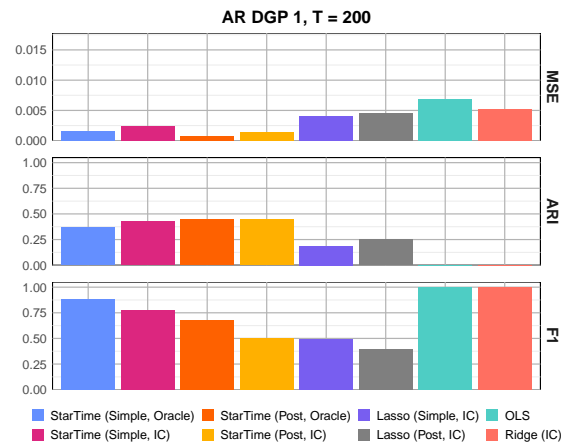
### 5.1.3 Results

The results for the AR simulations are shown in Figure 5. Across all DGPs and sample sizes, the StarTime estimators, particularly its post-selection variant, demonstrate strong performance in estimation accuracy, aggregation and sparsity recovery.

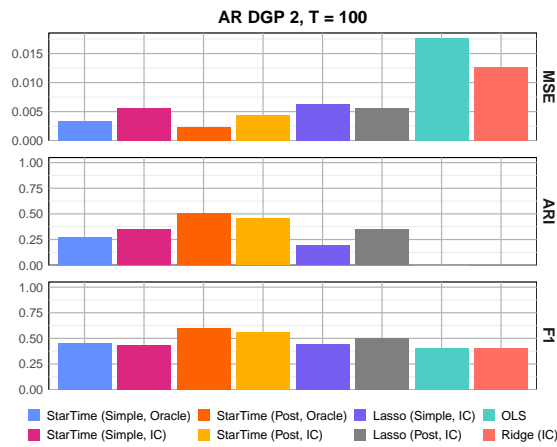
With respect to MSE, StarTime consistently outperforms OLS, Ridge, and Lasso, particularly in settings where the true DGP exhibits aggregation (DGP 1 and 2). In DGP 1 (aggregation without sparsity), Simple StarTime achieves lower MSE than competing methods, with Post StarTime displaying further improvements as the sample size increases. The performance gaps between the BIC and Oracle versions also tend to reduce as the sample size increases. Both OLS and Ridge perform poorly. Lasso, despite its inability to exploit the underlying aggregation structure, is the most competitive benchmark. When aggregation is combined with sparsity (DGP 2), the StarTime estimators maintain their advantage, achieving the lowest MSE values, with Post StarTime delivering the most accurate estimates. The performance of Lasso compared to StarTime improves, which is to be expected as it can now leverage the DGP’s sparsity. DGP 3 (sparsity without aggregation), naturally favors the Lasso; it performs very well. Still, Post StarTime (IC) matches the performance of Lasso (Post, IC), demonstrating StarTime’s flexibility in successfully identifying



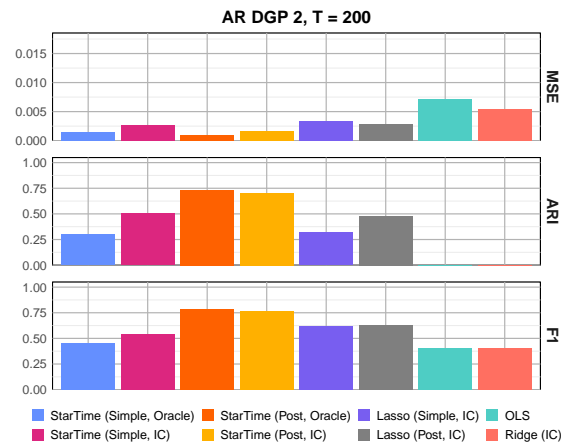
(a) DGP 1,  $T = 100$



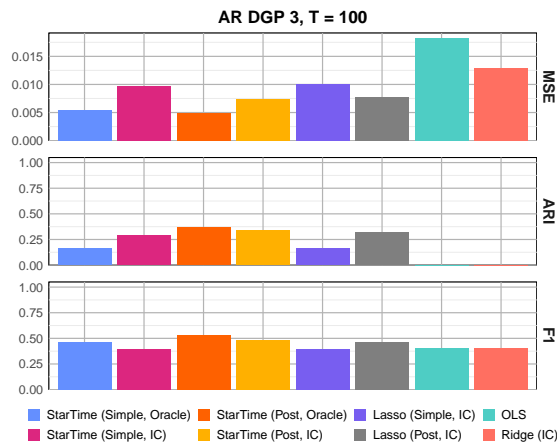
(b) DGP 1,  $T = 200$



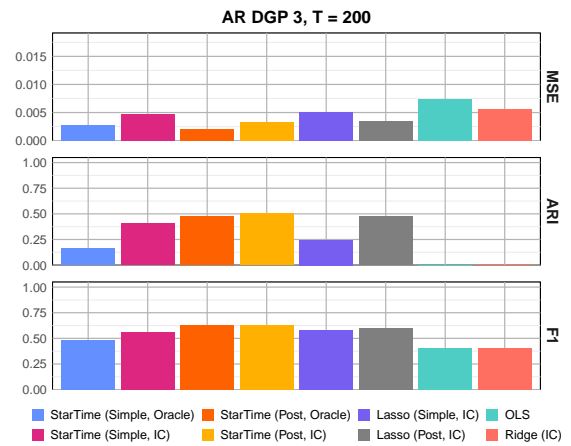
(c) DGP 2,  $T = 100$



(d) DGP 2,  $T = 200$



(e) DGP 3,  $T = 100$



(f) DGP 3,  $T = 200$

Figure 5: Performance metrics of the estimators across the three AR-based DGPs.

that sparsity, rather than aggregation, is the relevant simplicity structure to leverage.

Turning to aggregation recovery, StarTime, and especially Post StarTime, recovers the underlying aggregation structure in DGP 1 and DGP 2 most accurately. The low ARI is primarily attributable to StarTime’s tendency to merge the two most distant lagged groups into a single group instead. The ARI penalizes this type of clustering discrepancy severely; however, its effect on MSE remains limited. In DGP 3, where no true aggregation exists apart from the zero group, Post StarTime occasionally wrongly identifies groups, yet it still achieves the highest ARI, competitive to that of Post Lasso. As expected, OLS, Ridge, and the standard Lasso yield an ARI of zero across all DGPs as none of them are designed to induce a grouping structure.

Finally, regarding sparsity recognition, the F1 scores align with our expectations. In DGP 1, where all coefficients are non-zero, OLS and Ridge correctly refrain from penalizing parameters. Simple StarTime outperforms its post-selection variant in this setting, as the latter tends to over-penalize, introducing unnecessary shrinkage. However, this over-penalization is concentrated on more distant rather than recent lags, where coefficients are already close to zero, so the impact on MSE remains limited. In DGP 2, both StarTime and Post Lasso effectively identify zero coefficients, with Post StarTime demonstrating improved recovery as  $T$  increases. Finally, in DGP 3, the StarTime variants and Lasso variants exhibit very similar performance.

## 5.2 Mixed-Frequency DGPs

### 5.2.1 Data Generating Processes

We consider three mixed-frequency DGPs, similar to [Babii et al. \(2022\)](#). The response  $y_t$  is observed quarterly, the covariates  $x_h$  monthly; hence  $m = 3$ .

**DGP 1** is given by

$$y_{mt} = 0.3y_{m(t-1)} + 0.01y_{m(t-2)} + 0y_{m(t-3)} + 0y_{m(t-4)} + \sum_{i=1}^3 \sum_{j=1}^{12} \omega_j^{[i]} x_{mt-(j-1)}^{[i]} + \varepsilon_{mt}, \quad (11)$$

where we include an autoregressive component with two effective (non-zero) lags and three covariates with twelve monthly lags each. Each lag weight  $\omega_j^{[i]}$  is generated from a Beta distribution with parameters Beta(1,3), Beta(2,3), and Beta(2,2), respectively.

**DGP 2** is given by

$$y_{mt} = 0.3y_{m(t-1)} + 0.01y_{m(t-2)} + 0y_{m(t-3)} + 0y_{m(t-4)} + \sum_{i=1}^{10} \sum_{j=1}^{12} \omega_j^{[i]} x_{mt-(j-1)}^{[i]} + \varepsilon_{mt}, \quad (12)$$

where  $\omega_j^{[i]}$  is generated as in DGP 1 for the first three covariates and zero otherwise. DGP 2 is thus the same as DGP 1, but when estimating, we include the seven additional irrelevant covariates.

**DGP 3** is given by

$$y_{mt} = 0.3y_{m(t-1)} + 0.01y_{m(t-2)} + 0y_{m(t-3)} + 0y_{m(t-4)} + \sum_{i=1}^3 \bar{\omega}^{[i]} \sum_{j=1}^{12} x_{mt-(j-1)}^{[i]} + \varepsilon_{mt}, \quad (13)$$

where  $\bar{\omega}^{[i]} = \frac{1}{12} \sum_{j=1}^{12} \omega_j^{[i]}$  denotes the average of the monthly Beta weights for covariate  $i$ .

Across all DGPs, all covariates are generated as AR(1) processes  $x_h = 0.2x_{h-1} + \varepsilon_h$  with  $\varepsilon_h \sim \mathcal{N}(0, 1)$ , where  $h$  denotes the monthly frequency, and the errors  $\varepsilon_{mt} \sim \mathcal{N}(0, 1)$ . For DGP 3, we retain the same Beta distribution parameters but replace the unit-sum normalization with covariate-specific scaling, so that the weights of each covariate sum to different values.

### 5.2.2 Estimators

We compare StarTime to three benchmarks: *OLS*, *Restricted MIDAS* (Ghysels et al., 2004) and *MIDAS-ML* (Babii et al., 2022). OLS serves as a baseline estimator without penalization. Restricted MIDAS serves as a baseline estimator for mixed-frequency regressions. We use the implementation in the `midasr` package (Ghysels et al., 2016) with a normalized Almon lag polynomial using parameters  $(1, -0.5)$ . MIDAS-ML serves as a sparse benchmark estimator for mixed-frequency regressions which allows for variable selection in high-dimensional mixed-frequency regressions. We use the default implementation in the `midasm1` package (Striaukas et al., 2022).

For StarTime, we use the tree structures in Figure 4 for the monthly covariates and the quarterly one. For both DGP 1 and DGP 2, the tree structure is misspecified, since the natural groupings implied by the Beta-distributed weights do not align perfectly with the tree hierarchy. In contrast, DGP 3 constructs covariate weights by averaging the Beta-generated lag weights within each covariate, assigning a common coefficient to all lags of a given covariate. The tree structure can capture such temporal aggregation. As in Section 5.1, we report results for the Oracle and BIC-based selection of the tuning parameters. For the BIC, we set  $c = 1$  in DGP 1 and 3 but lower it to  $c = 0.5$  in DGP 2 with  $T = 100$  to reduce the risk of overfitting (Chen and Chen, 2012) since the number of parameters ( $N = 124$ ) exceeds the sample size. This adjustment limits the maximum number of non-zero estimated parameters to 62, which still allows the model to capture key signals.

### 5.2.3 Results

The results for the mixed-frequency simulations are shown in Figure 6. In terms of Mean Squared Error, distinct performance profiles emerge depending on the structure of the lag weights. In DGP 1, characterized by Beta-distributed weights without explicit aggregation, MIDAS and the Oracle-tuned StarTime perform best. The smooth Beta constraints of MIDAS are well-suited to this structure. The BIC-tuned StarTime slightly outperforms MIDAS-ML, suggesting that StarTime remains competitive even when the true DGP lacks the tree-based aggregation structure it is designed to exploit. Post StarTime exhibits a slightly higher MSE than the Simple StarTime, due to the more pronounced imposition of temporal aggregation where none exist. The performance gap between BIC and Oracle-based tuning widens as the dimensionality increases.

In the high-dimensional setting of DGP 2, the limitations of unpenalized methods are apparent. For  $T = 100$ , where the number of parameters exceeds the sample size, OLS is infeasible. For  $T = 200$ , OLS yields a substantially higher MSE than the penalized methods, including StarTime, which maintain robust performance. Finally, in DGP 3, where the weights exhibit a clear aggregation structure, the StarTime estimators perform best, as expected. MIDAS-ML performs considerably worse: Its MSE is 0.115 for  $T = 100$  and 0.006 for  $T = 200$ ; for clarity of presentation, the vertical axis is capped. MIDAS-ML appears sensitive to the chosen lag structure when it does not align with its smoothness restrictions across the lags. In contrast, StarTime remains competitive in DGP 1 and 2 to MIDAS-ML, even when relying on a misspecified tree structure.

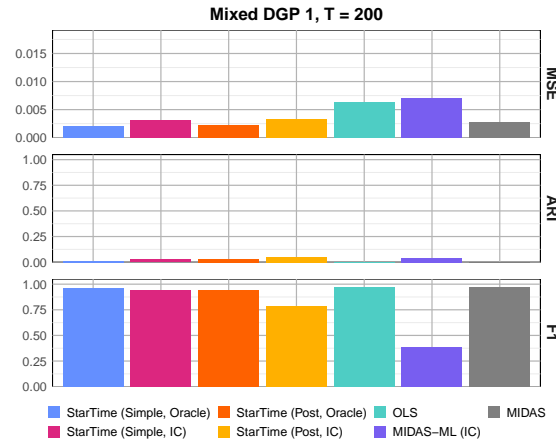
Regarding aggregation recovery, OLS yields a zero ARI across all simulations, as expected. In DGP 1, all ARIs are low since there is no aggregation to uncover. In DGP 2, the only relevant grouping structure that can be uncovered is the separation of the ‘group’ of irrelevant covariates from the relevant ones. The StarTime estimators best capture this separation. In DGP 3, where temporal aggregation is present, the StarTime estimators stand out as the strongest performers.

Regarding sparsity recovery, in DGP 1, where nearly all coefficients are non-zero, all methods apart from MIDAS-ML achieve high F1 scores. In DGP 2, where 7 irrelevant covariates are added compared to DGP 1, StarTime and especially its post-selection variant demonstrate superior performance. The refitting step considerably improves sparsity recovery, especially in high-dimensional settings where the signal is weaker. In DGP 3, where coefficients feature strong aggregation but minimal sparsity, all methods consistently achieve excellent recovery rates, especially for  $T = 200$ .

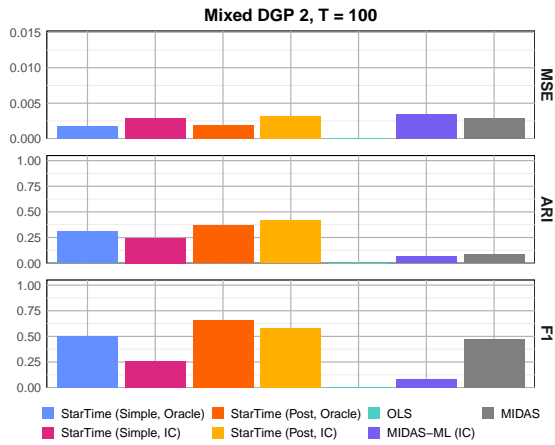
Overall, across both autoregressive and mixed-frequency DGPs, the StarTime estimators demonstrate strong performance in terms of estimation accuracy, aggregation and sparsity recovery compared to alternatives. They adaptively emphasize aggregation or sparsity in line with the underlying



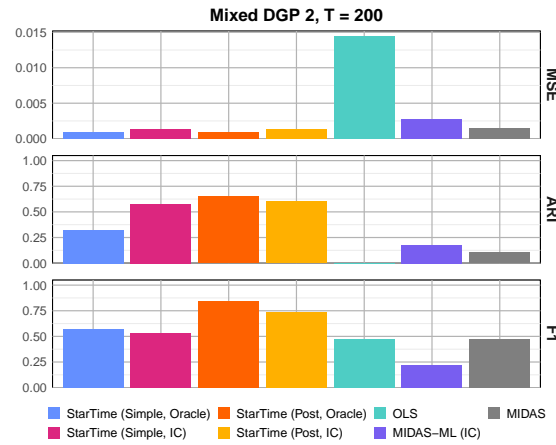
(a) DGP 1,  $T = 100$



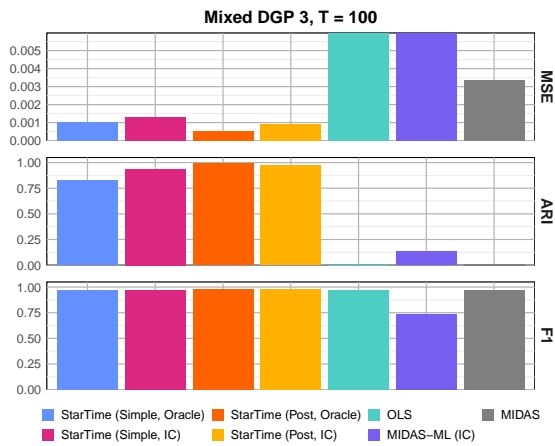
(b) DGP 1,  $T = 200$



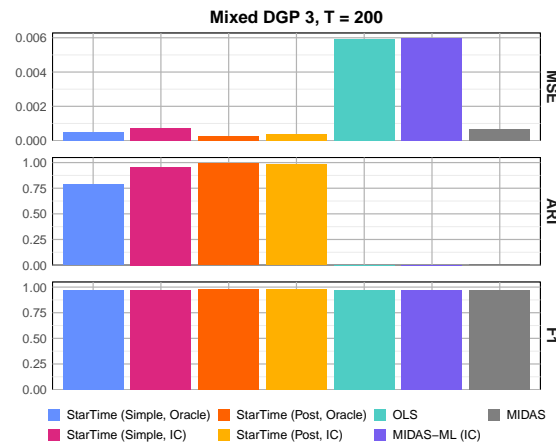
(c) DGP 2,  $T = 100$



(d) DGP 2,  $T = 200$



(e) DGP 3,  $T = 100$



(f) DGP 3,  $T = 200$

Figure 6: Performance metrics of the estimators across the three mixed-frequency DGPs.

DGP. Even when the temporal tree structure is misspecified, StarTime remains competitive.

## 6 Empirical Applications

We demonstrate the versatility of StarTime on two empirical applications: One on realized volatility forecasting (Section 6.1) and another on macroeconomic nowcasting and forecasting (Section 6.2).

### 6.1 Financial Application

#### 6.1.1 Realized Variance Forecasting

We apply our method to realized variance forecasting. The simple and parsimonious HAR model by Corsi (2009) is known to perform extremely well; it consistently outperforms a range of statistical and machine learning approaches (Chassot and Audrino, 2026). The HAR relies on a fixed temporal aggregation structure grounded in financial knowledge, reflecting the investment horizons of different investors. Our goal is not to outperform the HAR in terms of forecasting ability. While StarTime contains the HAR as a special case, it does not impose the HAR’s aggregation structure a priori. Instead, it allows for multiple levels of temporal aggregation across a richer lag space, potentially combined with sparsity. Using StarTime, we aim to provide data-driven evidence on whether the HAR’s aggregation structure is supported across a wide range of stocks and fitting schemes. We employ the realized variance dataset from Hecq et al. (2023) which consists of 10-min realized variances (RV) from March 20th, 2008 to February 17th, 2017 ( $T = 2236$  trading days) for a set of 30 major U.S. financial assets.<sup>2</sup> Appendix B contains an overview of the considered stocks.

#### 6.1.2 Model and Benchmarks

Following standard practice in the literature, we model the logarithmic transformed realized variance,  $y_t = \log(RV_t)$ . We consider an autoregressive forecasting model where  $y_{t+h}$  is predicted using  $N$  lags of  $y_t$ . We focus on forecast horizons of  $h = 1$  (one day),  $h = 5$  (one week), and  $h = 20$  (one month) and use a direct forecast approach.

For the StarTime estimators, we specify a maximum lag length of  $N = 20$  days, corresponding to approximately one trading month, and use the HAR-inspired tree structure in Figure 3. We also perform robustness checks allowing for a deeper history of  $N = 40$  lags, using a tree that aggregates the 40 daily lags into 8 weekly groups (each containing 5 days), which are then aggregated into two monthly groups, and a single ‘two-month’ root.

---

<sup>2</sup>High-frequency stock data for constructing the realized variances was kindly provided to us by M.C. Medeiros.

We compare StarTime against three benchmarks: The HAR model, a simple AR(1), and a Random Walk. The HAR model given by

$$y_{t+h} = \beta_0 + \beta^{(d)}y_t + \beta^{(w)} \left( \frac{1}{5} \sum_{j=1}^5 y_{t-j+1} \right) + \beta^{(m)} \left( \frac{1}{20} \sum_{j=1}^{20} y_{t-j+1} \right) + \epsilon_{t+h}. \quad (14)$$

To evaluate the performance of the methods across different fitting schemes, we employ a rolling window approach. For forecast horizon  $h$ , we fix the window size at  $W - h + 1$  and consider  $W \in \{125, 250, 1000\}$ , corresponding approximately to one semester, one year, and four years of trading days respectively. As commonly done for penalized estimators, we standardize the response in each rolling window to have zero mean and unit variance. We tune the parameters  $\lambda_1$  and  $\lambda_2$  for StarTime in each rolling window using the BIC with  $c = 1$ .

### 6.1.3 Evaluation Metrics

We evaluate out-of-sample forecasting performance using two widely used loss functions: Mean Squared Error (MSE) and Quasi-Likelihood (QLIKE) loss. While the MSE is a symmetric loss, the QLIKE is asymmetric and more robust to extreme outliers, making it particularly suitable for volatility evaluation ([Patton, 2011](#)). For  $N_{test}$  out-of-sample forecasts, the QLIKE is defined as:

$$\text{QLIKE} = \frac{1}{N_{test}} \sum_{t=1}^{N_{test}} \left( \frac{\exp(y_t)}{\exp(\hat{y}_t)} - \log \left( \frac{\exp(y_t)}{\exp(\hat{y}_t)} \right) - 1 \right).$$

Since we forecast the log-variance  $y_t$ , we exponentiate the forecasts and actuals to compute the QLIKE on the original scale of realized variances, consistent with [Chassot and Audrino \(2026\)](#).

We assess forecast accuracy using the Diebold-Mariano (DM) test ([Diebold and Mariano, 1995](#)) for pairwise comparisons and the Model Confidence Set (MCS, [Hansen et al., 2011](#)) for multi-model evaluation. For the DM tests, implemented in the `forecast` package ([Hyndman and Khandakar, 2008](#)), we test the null of equal predictive accuracy between Post StarTime and each benchmark for every asset. The tests are conducted at the 5% significance level. We summarize results by reporting the Win Rate and Loss Rate across stocks for each configuration. The Win Rate is the percentage of stocks where Post StarTime significantly outperforms the benchmark ( $p$ -value  $< 0.05$  and test statistic  $< 0$ ). The Loss Rate is the percentage of stocks where Post StarTime significantly underperforms ( $p$ -value  $< 0.05$  and test statistic  $> 0$ ). The remaining proportion represents cases where the models are statistically indistinguishable (ties). For the MCS evaluation, we use the  $T_{max}$  statistic with  $B = 5000$  bootstrap replications and  $\alpha = 0.05$ , implemented in the package

MCS (Bernardi and Catania, 2018). We report the MCS inclusion rate, defined as the percentage of stocks for which a method is included in the final MCS.

#### 6.1.4 Results

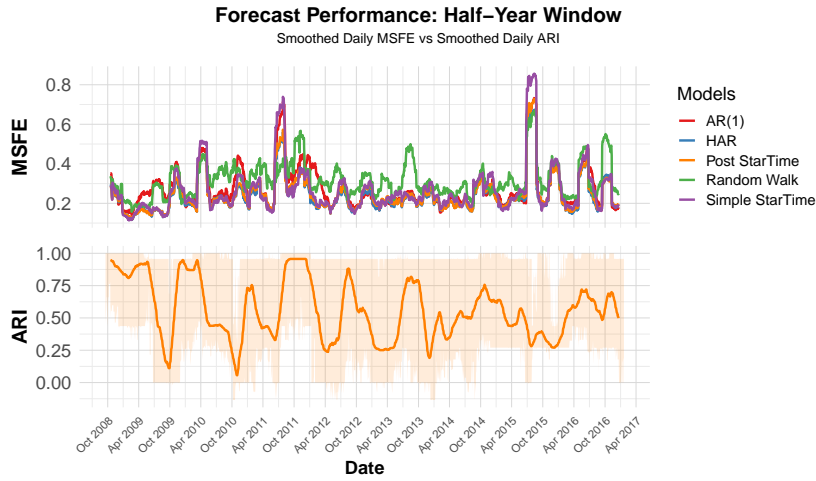
Figure 7 summarizes the results for horizon  $h = 1$  and different fitting schemes across the panels. We display the MSFE, averaged across stocks, over time for the five methods. We also compute the ARI that compares the grouping structure of Post StarTime with that of the HAR. Since the raw daily results are rather noisy, we use a centered moving average filter to smooth the results for visual purposes: For a chosen window size  $S$ , the smoothed value at time  $t$  is computed as the simple average of observations in the interval  $[t - \lfloor S/2 \rfloor, t + \lfloor S/2 \rfloor]$ ; we use  $S = 20$ .

We first examine the MSFE curves for the one-step-ahead forecast horizon ( $h = 1$ ) in the 20-lag configuration. While the HAR model unsurprisingly remains the overall best performer, both Simple and Post StarTime track its performance closely. Simple StarTime occasionally exhibits high error peaks, especially in the July–October 2015 period. This instability is effectively mitigated by Post StarTime which offers the distinct advantage of producing more parsimonious, aggregated estimates. In contrast, the AR(1) benchmark and, most notably, the Random Walk exhibit higher errors throughout the sample period.

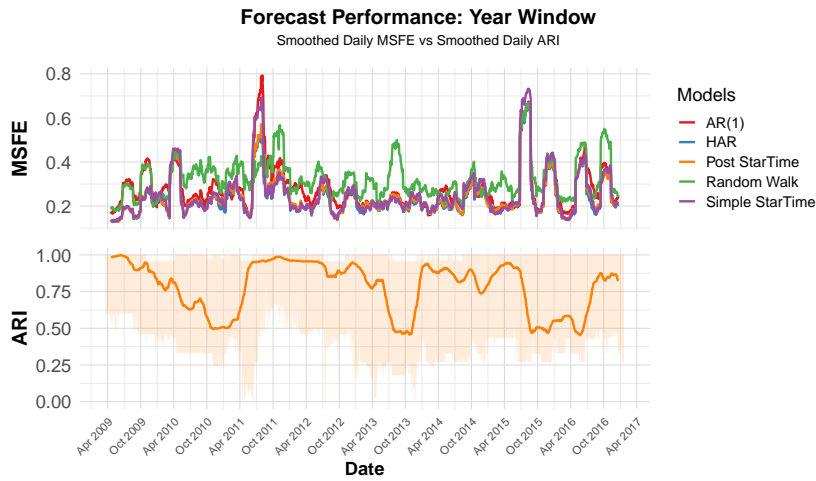
The MCS results (Table 3, Appendix C) confirm that the HAR is the best performer. Its dominance is, however, less pronounced for  $h = 20$  compared to  $h = 1$  and  $h = 5$ . Indeed, the inclusion rate of the StarTime estimators increases as the forecast horizon and/or the window size increases. The AR(1) is competitive for longer horizons. The Random Walk yields the worst performance, a result consistent with the known mean-reverting properties of volatility, which the Random Walk fails to capture at such short horizons (Poon and Granger, 2003).

The Diebold-Mariano (DM) tests, detailed in Table 4 of Appendix C, further confirm that the HAR model performs, overall, best for horizon  $h = 1$ . The StarTime estimators are competitive to the HAR for longer horizons, suggesting that our data-driven tree-based aggregation effectively captures longer-run dynamics. Post StarTime consistently outperforms the Random Walk and AR(1), and outperforms or matches Simple StarTime for next-day forecasts under MSFE loss.

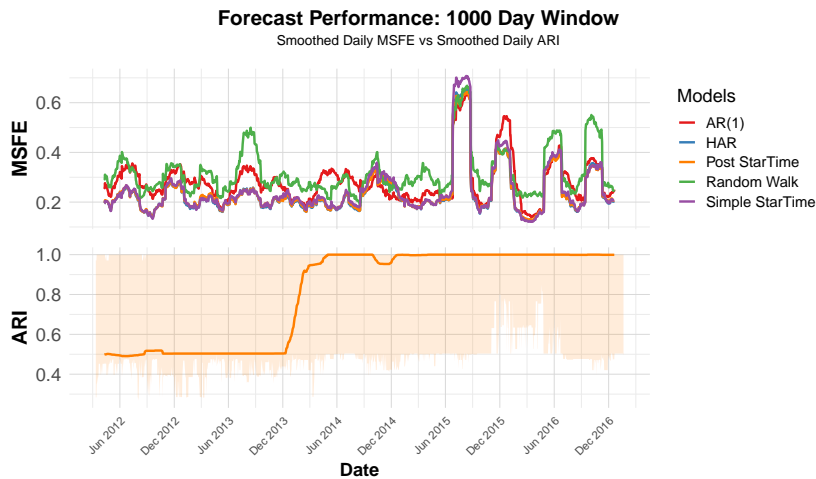
Next, we turn to the ARI curves in Figure 7. The results for the 1000-day window demonstrate most stability: The median ARI never falls below 50% and remains steadily around one from May 2014 onward. Even for the 250-window size, the ARI mostly fluctuates between 0.5 and 1. Figure 8 further confirms that StarTime provides data-driven support for the HAR lag structure. The heatmaps for two stocks, Nike Inc. and JPMorgan Chase &Co, visualize the temporal aggregation



(a) 125 Day-window, horizon 1, 20 lags included

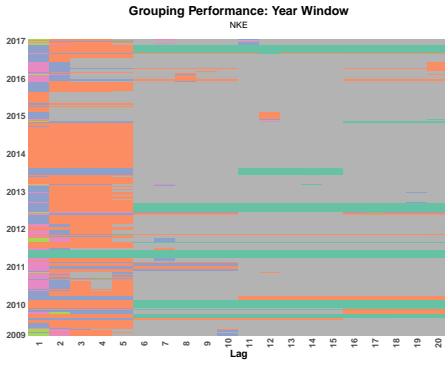


(b) 250 Day-window, horizon 1, 20 lags included

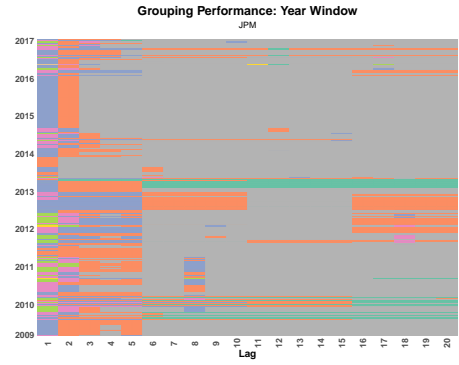


(c) 1000 Day-window, horizon 1, 20 lags included

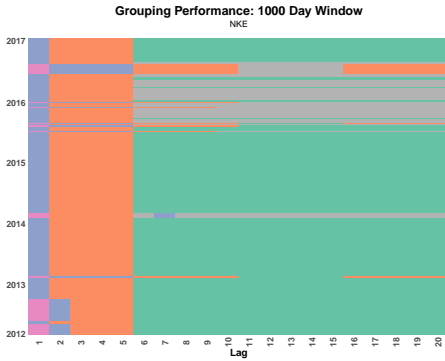
Figure 7: Comparative forecast performance across varying fitting schemes. Each panel displays the smoothed daily median MSFE (top) and smoothed daily median ARI (bottom). Shaded regions in the ARI plots represent the 10<sup>th</sup> and 90<sup>th</sup> percentiles.



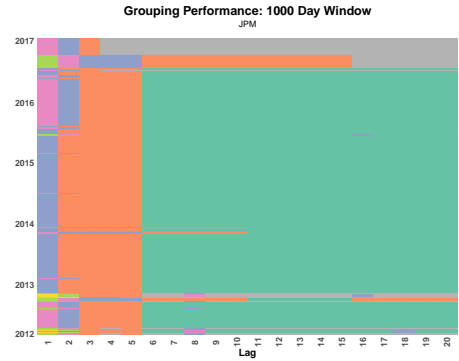
(a) 250 Day-window, Nike Inc.



(b) 250 Day-window, JPMorgan Chase & Co.



(c) 1000 Day-window, Nike Inc.



(d) 1000 Day-window, JPMorgan Chase & Co.

Figure 8: Rolling-window coefficient heatmaps for Post StarTime (horizon 1, 20 lags) applied to Nike Inc. (NKE) and JPMorgan Chase & Co (JPM), with window sizes of 250 and 1000 trading days, respectively. Each row indexes an estimation date, while columns correspond to daily lags  $j = 1, \dots, 20$ . Cell colors encode the aggregation structure selected by Post StarTime: Lags assigned identical colors have been fused into a single coefficient group through the tree-guided penalty, distinct colors within a row reflect heterogeneous lag effects retained at the daily frequency, and coefficients set to zero are indicated in gray.

structure recovered by Post StarTime. Without a priori imposing the HAR-based structure, it is oftentimes exactly recovered across the vast majority of time points, especially so for the 1000-window fitting scheme. The half-year window displays a more volatile heatmap, even though the HAR-based structure still shines through.

Detailed results for the QLIKE loss are included in Tables 5 and 6 of Appendix C. Overall, the same conclusions as for the MSFE loss hold; we highlight the differences. The Random Walk model occasionally appears in the MCS, but the pairwise DM-tests indicate that it never statistically outperforms Post StarTime. Besides, when comparing StarTime with the AR(1) model using the QLIKE loss, the former is generally favored overall; however, the latter remains particularly robust at longer horizons, as it is consistently included in the QLIKE MCS for  $h = 20$ .

Finally, the above findings largely extend to the configurations with 40 lags, see Tables 3 to 6 in Appendix C. A notable difference occurs for the QLIKE loss, where the AR(1) tends to outperform StarTime. The inclusion of 20 additional lags substantially increases the dimensionality of the lag

space, which inherently complicates lag selection and aggregation by StarTime, especially in smaller rolling window fitting schemes. Since the HAR structure (i.e., the first 20 lags) already captures volatility dynamics well, additional lags may be redundant. While the AR(1) avoids this overfitting by design, StarTime’s performance hinges on shrinking these distant lags to zero. The aggregation patterns for individual stocks confirm this: For  $W = 1000$ , StarTime removes the 20–40 daily lags and maintains its accuracy. In smaller windows, however, it struggles to consistently eliminate these distant lags, resulting in a performance dip relative to the parsimonious benchmarks. When domain knowledge about the appropriate lag length is available, we advise incorporating this directly rather than relying on an excessively large lag space.

Overall, our findings suggest that StarTime remains a strong and flexible estimator that offers data-driven evidence that the HAR’s temporal aggregation structure is strongly supported across a wide range of stocks, particularly for larger window sizes.

## 6.2 Macroeconomic Application

### 6.2.1 Nowcasting and Forecasting GDP Growth

We now evaluate StarTime’s ability to nowcast and forecast GDP growth using mixed-frequency economic and financial time series. We construct a comprehensive dataset spanning from 1992:Q2 to 2025:Q2 that captures a broad overview of the US economy. The dataset comprises 30 variables covering diverse economic categories: Market indices, economic uncertainty policy, financial indicators, labor market metrics, income and sales, capacity utilization, prices, housing, and production inventories. Our variable selection is grounded in economic theory and inspired by recent mixed-frequency literature (Striaukas et al., 2022; Hecq et al., 2022). The raw series are collected from the FRED database, Yahoo Finance, and the Policy Uncertainty website (Baker et al., 2026).

We transform the variables following the transformation codes in FRED-MD (McCracken and Ng, 2016) and FRED-QD (McCracken and Ng, 2021). For financial and uncertainty series not covered therein, we apply logarithmic transformations when supported by the literature: We use the log of the Economic Policy Uncertainty (EPU) index (Baker et al., 2016) and the log of the VIX (Andersen et al., 2003; Taylor, 2019). The National Financial Conditions Index (NFCI) enters the model in levels, consistent with Amburgey and McCracken (2023). For any remaining variables, unit root tests are conducted using the `bootUR` package (Smeekes and Wilms, 2023) to determine the appropriate order of integration. Appendix D contains a detailed overview of the considered variables, their sampling frequency, seasonal-adjustment status, and the applied transformations. We include all series at the highest sampling frequency available across sources, and use StarTime to

provide data-driven guidance on the appropriate temporal aggregation level at which each variable should enter the model.

### 6.2.2 Model and Benchmarks

We consider the mixed-frequency model (1) with quarterly GDP growth as response and daily, weekly, monthly and quarterly covariates. We use a lag structure that spans the previous full quarter and set  $m = 60$ . For the daily covariates, we include 60 lags (spanning approximately 3 months of 20 trading days), for the weekly covariates, we include 12 lags (spanning approximately 12 weeks per quarter), for the monthly variables, we include 3 lags and for the quarterly variables we include one lag. The full model contains 5 daily, 3 weekly, 20 monthly, and 2 quarterly regressors (including the response), yielding a total of  $N = 398$  predictors. We also consider a ‘reduced’ model to evaluate performance in a more parsimonious setting: It contains  $N = 49$  predictors; 2 weekly and 8 monthly core variables alongside the GDP lag (see Tables 7 to 10 of Appendix D).

*Remark 3.* All series are aligned to the quarterly forecast target. Weekly variables require specific attention, as they do not map cleanly into months or quarters. To prevent look-ahead bias, we employ a hard assignment rule based on the week-ending Saturday: A week is attributed to a specific quarter only if its Saturday falls within that quarter. This ensures that a week straddling two quarters is assigned to the period where it ends.

Model (1) allows us to forecast GDP growth for the next quarter. We also consider a nowcasting set-up where we include lags of the daily, weekly and monthly covariates within the ongoing quarter; hence using lags  $x_{mt-m_i(j-1)}$  instead of  $x_{m(t-1)-m_i(j-1)}$  for those covariates  $i$  with  $m_i < m$  in model (1). We employ a rolling window approach with window sizes  $W \in \{66, 105\}$ , corresponding to approximately 50% and 80% of the sample, respectively. Within each window, all predictors and the target variable are standardized to have zero mean and unit variance.

For the StarTime estimators, we specify one temporal tree per regressor, which constitutes a high-dimensional extension of the multiple tree-structure illustrated in Example 4. For daily regressors, the tree starts from 60 leaves, which are aggregated into 12 weeks of 5 days, then into 3 ‘months’ of 4 weeks, and finally into a single quarterly node. Weekly trees follow the same logic, but start directly from 12 weekly lags, which can be aggregated into 3 month-level nodes and then into one quarterly node. Monthly trees have two levels, with 3 monthly lags aggregated into a quarter, while quarterly regressors are represented by a single-node tree.

We tune  $\lambda_1$  and  $\lambda_2$  for StarTime in each rolling window using the BIC with  $c = 0.3$ . Due to the pronounced high-dimensionality of the full model, the regularization grid may, however, contain

a large region of tuning parameter values that yield too complex models. To address this, we implement a two-step grid construction: We start with the initial grid, then redefine the grid by restricting  $\lambda_1$  and  $\lambda_2$  to the empirically relevant range (between the largest and smallest values that yield admissible solutions according to the threshold  $c$ ), and re-estimate on this refined grid.

We then benchmark the forecast performance of StarTime, in terms of Mean Squared Forecast Error, against three alternatives: The Random Walk and AR(1) serve as standard forecast baselines but they cannot deliver a nowcast. We therefore also compare our approach to MIDAS-ML (Striaukas et al., 2022), a state-of-the-art method for high-dimensional mixed-frequency regressions that also utilizes penalization and leans itself well to a nowcast and forecast set-up. As in the simulation study, MIDAS-ML is implemented using the `midasm1` package with default settings, specifically we set the mixing parameter to one which corresponds to a sparse-group Lasso.

*Remark 4.* A fully fledged nowcasting exercise requires explicitly accounting for real-time data vintages and data revisions. We deliberately adopt a simplified nowcasting framework to isolate and illustrate the potential of StarTime in a nowcast-versus-forecast setting. For a fair comparison, we impose the same setup for both StarTime and MIDAS-ML. While this simplified set-up is informative in its own right, the results should be interpreted accordingly. Extending to a full real-time nowcasting exercise is feasible within our framework but beyond the scope of the paper.

### 6.2.3 Results

Figure 9 summarizes the evolution of the MSFEs for the nowcasting and the forecasting set-up on the reduced model for  $W = 105$ . Across all forecast methods, the reduced model results in lower overall MSFEs than the full model. This result underwrites the value of careful, economically grounded pre-selection of relevant predictors. Detailed results on the full model ( $W = 105$  and  $W = 66$ ) and the reduced model ( $W = 66$ ) are available in Figures 10, 11, and 12 in Appendix E.1.

The plots show a clear spike in forecast errors around 2020, corresponding to the onset of the COVID-19 pandemic. We formally define this COVID period as spanning 2020:Q1 to 2021:Q4, identified by locating where the maximum squared residual across all evaluated models exceeded five times the sample median. The simple benchmarks (Random Walk and AR(1)) produce notably larger forecast errors during the COVID period than StarTime and MIDAS-ML (Figure 9, panel b). Incorporating high-frequency information thus yields clear gains for forecast accuracy. Moreover, nowcast errors are generally smaller than forecast errors (Figure 9, panel a versus b), as expected, since nowcasts exploit additional information that becomes available within the forecast horizon. Outside of the pandemic period, the models behave very similarly; differences in accuracy are small

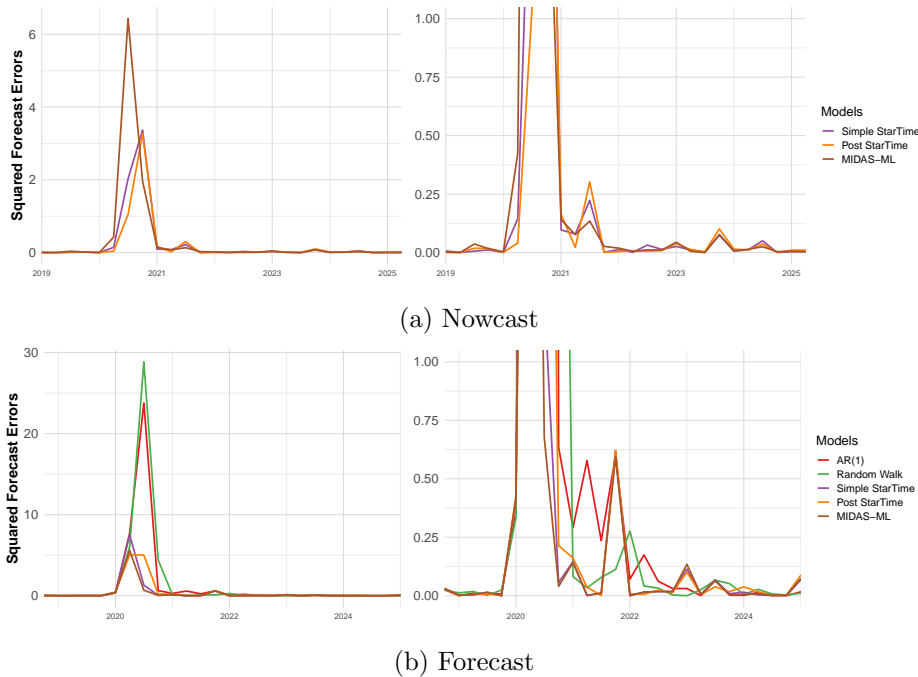


Figure 9: Evolution of squared forecast errors for the Reduced Set (49 predictors) with  $W = 105$ . Both (a) and (b) include a censored zoom to account for COVID-19 volatility. The plotted squared forecast errors are multiplied by 1000 due to the small scale of GDP growth.

and do not persist after 2022.

We evaluate nowcast and forecast accuracy in more detail using the MSFEs reported in Table 1 for  $W = 105$ . The results for  $W = 66$  are largely similar and available in Table 11 of Appendix E.2. The nowcasts ( $h = 0$ ) from Post StarTime achieve the lowest MSFE across the total out-of-sample period for the reduced model, followed by the  $h = 0$  results for Simple StarTime and MIDAS-ML. Post StarTime nowcasts outperform Post StarTime forecasts by 56%; this result is intuitive since the nowcasting model set-up explicitly leverages high-frequency inter-quarter information. A surprising result, at first sight, is that MIDAS-ML forecasts lead to a lower MSFE than its nowcasts. However, this is largely driven by the COVID-peak, during which MIDAS-ML seems to struggle to handle the extreme volatility. Post StarTime nowcasts are 45% lower than the ones from MIDAS-ML during the COVID peak. Outside of the COVID-peak, MIDAS-ML nowcasts do perform better than its forecasts. In fact, its nowcasts perform best and are closely followed by StarTime and Post StarTime. Finally, the benchmarks AR(1) and Random Walk are not competitive during the COVID-peak. Outside the COVID-peak, the forecast performances of the AR(1) and Random Walk get considerably closer to the forecast results of the mixed-frequency models.

To assess whether the differences in nowcast and forecast performance are statistically significant, we compute the MCS for  $W = 105$  and  $W = 66$  separately, the results are available in Tables 12 to 15 of Appendix E.2. No single model dominates. We find the same conclusion when com-

Table 1: MSFE for window  $W = 105$ 

	Post StarTime		Simple StarTime		MIDAS-ML		AR(1)	Random walk
	$h = 0$	$h = 1$	$h = 0$	$h = 1$	$h = 0$	$h = 1$		
<i>Reduced Set</i>								
Total	0.198	0.459	0.239	0.401	0.365	0.302	1.336	1.561
Non-peak	0.017	0.023	0.015	0.022	0.015	0.022	0.029	0.035
COVID-peak	0.607	1.442	0.744	1.254	1.152	0.933	4.277	4.994
<i>Full Set</i>								
Total	0.332	0.342	0.695	0.664	0.749	0.356	1.336	1.561
Non-peak	0.044	0.036	0.056	0.027	0.018	0.028	0.029	0.035
COVID-peak	0.981	1.031	2.134	2.096	2.395	1.094	4.277	4.994

*Note: MSFE values are multiplied by 1000 due to the small scale of GDP growth.*

putting the MCS for the off-peak out-of-sample period only. The general difficulty in significantly outperforming univariate baselines for forecasting GDP growth is a well-known result. Parsimonious autoregressive benchmarks are particularly robust for stationary series like GDP growth, often proving difficult to beat even with sophisticated structural or high-dimensional models (e.g., [Stock and Watson, 2007](#); [Marcellino et al., 2006](#)). This aligns with our observation that especially the off-peak performance of simple models is competitive to that of the more complex models.

While Post StarTime performs competitively in terms of MSFE, it uncovers economically interpretable structures through its temporal aggregation and sparsity, thereby facilitating a clearer understanding of the underlying drivers of its nowcast/forecast performance. We analyze the structure of the coefficients estimated by Post StarTime in more detail. We observe differences between the full and restricted model set-up, as well as between the nowcasting and forecasting exercises. In the high-dimensional full forecasting model, StarTime primarily utilizes sparsity to handle the large parameter space, with almost no aggregation. In contrast, within the reduced set, the model frequently exploits temporal fusion, aggregating high-frequency lags into coarser ones. StarTime typically yields denser coefficient vectors for the nowcast specifications than the forecast one, reflecting that more high-frequency covariates are retained among the intra-quarter information. Since StarTime performs best on the reduced model set-up, we focus our discussion on these results.

Temporal aggregation is most pronounced in the housing, financial, and manufacturing variables. For instance, in the  $W = 105$  window, the monthly log-levels of New Privately-Owned Housing Units Authorized (log PERMIT) are fully aggregated to a single quarterly lag across 65% of the rolling windows for the nowcasts and even 96% for the next quarter forecasts. This finding aligns with the economic intuition that housing permits represent a pipeline of future activity; aggregating the monthly volatility reveals the persistent trend that drives quarterly GDP ([Cheung](#)

and Granovsky, 2016; Cortes and LaPoint, 2024). Similarly, the weekly Chicago Fed National Financial Conditions Index (NFCI) is aggregated 91% of the time for the  $W = 66$  nowcasts window, and 80% of the time for the forecasts. As noted by Brave and Butters (2011), while financial stress can be volatile at high frequencies, it is the persistent tightening of conditions over the course of a quarter that materially impacts real output, supporting StarTime’s choice to smooth these signals to a quarterly frequency. Furthermore, in the reduced nowcasting set ( $W = 105$ ), the Value of Manufacturers’ New Orders (AMTMNO) is fully aggregated 96% of the time. Smoothing the intrinsic volatility of new orders helps extract the underlying signal of industrial demand, reinforcing its established role as a stable leading indicator of aggregate output (Zarnowitz, 1992).

The sparsity patterns selected by StarTime reveal which predictors contain unique and relevant information for GDP growth, showcasing distinct lag preferences between nowcasting and forecasting. The first lag of quarterly GDP growth,  $\Delta \log(\text{GDP})_{t-1}$ , is selected in 69% of the nowcasts, indicating that persistence in GDP growth provides a useful baseline for assessing current-quarter activity, consistent with standard dynamic factor nowcasting models (Giannone et al., 2008). The nowcasting set-up also reveals a distinct ‘anchoring’ behavior heavily reliant on early-quarter data. For variables like Nonfarm Payrolls (PAYEMS), Retail Sales (RSAFS), and Industrial Production (INDPRO), the nowcasting model predominantly selects their third lag, representing the earliest month of the quarter, over more recent releases. For example,  $\text{PAYEMS}_{t-3}$  is retained 100% of the time (with subsequent lags at 85%), and similarly,  $\text{INDPRO}_{t-3}$  is always retained (with  $\text{INDPRO}_{t-1}$  and  $\text{INDPRO}_{t-2}$  kept only 35% of the time). This structural choice suggests that early-quarter information establish the primary foundation for the trajectory of the quarter, while subsequent intra-quarter releases serve merely as marginal adjustments.

For the forecast model set-up with  $W = 105$ , an interesting selection pattern appears for the labor market variables. We observe the following structural difference between employment and jobless claims: While the model selects the first lag of Nonfarm Payrolls ( $\text{PAYEMS}_{t-1}$ ) in 84% of the cases, ignoring subsequent lags, it favours the second lag of Initial Claims ( $\text{ICSA}_{t-2}$ , 73%) over the first (35%). This data-driven insight aligns with the chronological classification of business cycle indicators established by Stock and Watson (1989): Payrolls act as a coincident indicator, where the most recent momentum is most predictive, whereas initial claims serve as a leading indicator, where signals often precede output changes by several months. Similarly, the model exhibits a preference for specific real-activity indicators, classified as ‘hard data’ by Giannone et al. (2008) for their high information content. For Retail Sales (RSAFS), the first lag is consistently selected (with subsequent lags excluded), capturing the immediate impact of consumption news. Conversely, for Industrial

Production (INDPRO), both the first and second lags are retained (100% and 54%, respectively). This difference likely reflects the distinct nature of these series: While sales data is volatile and its predictive content dissipates quickly, industrial production exhibits greater persistence, leading the model to use multiple lags to capture the underlying trend.

Finally, although StarTime’s high-dimensional full model-set exhibits lower accuracy than its reduced model set-up, it still offers several noteworthy insights. In particular, it also exhibits a preference for specific real-activity indicators. For  $W = 105$  and one-quarter-ahead forecast, the first lags of Industrial Production growth ( $\Delta \log(\text{INDPRO})$ ) and Real Manufacturing and Trade Sales ( $\Delta \log(\text{CMRMTSPL})$ ) are retained 100% of the time. Alongside these, Housing Sales (HSN1F), Retail Sales (RSAFS), and Payrolls (PAYEMS) all exhibit retention rates exceeding 90%. This selection mirrors the variables identified by the [NBER Business Cycle Dating Committee \(2025\)](#) as primary coincident indicators ([Stock and Watson, 1989](#)). Furthermore, the near-certain retention of housing sales underscores the critical role of the housing sector as an early warning system ([Leamer, 2007](#)). In the corresponding nowcasting full model set-up, additional distinct patterns emerge. The NFCI remains highly aggregated (88%), confirming the robustness of persistent financial signals. Notably, Total Business Inventories (BUSINV) are temporally grouped 81% of the time for  $W = 105$ , but in terms of sparsity, its second lag is consistently retained more frequently than its first or third lags across both window sizes. Inventories are heavily procyclical yet notoriously volatile and difficult to nowcast ([Blinder and Maccini, 1991](#)). The preference for the mid-quarter inventory lag suggests the model isolates this intermediate intra-quarter data point to gauge turning points in the inventory cycle before the quarter concludes. In the most high-dimensional setting ( $W = 66$ ), the nowcasting model strictly filters information to manage the acute dimensionality:  $\text{RSAFS}_{t-3}$  is retained 35% while its first two lags are ignored entirely, and similarly, only the third lag of CMRMTSPL is selected. This strict selection reinforces the notion that in high dimensions, early-quarter releases contain the most valuable information for predicting concurrent output.

Overall, StarTime achieves competitive nowcast and forecast performance relative to the considered benchmarks, while uniquely offering data-driven insights into the sampling frequency at which high-frequency variables are most relevant for modeling GDP growth.

## 7 Conclusion

We propose a tree-structured penalized aggregation method to reduce dimensionality in high-order autoregressions and mixed-frequency regressions. Our estimator, StarTime, flexibly selects coeffi-

cients to be temporally aggregated at varying frequencies, or sparse, or a combination of both, as supported by the data. We establish its theoretical properties by deriving an error bound under very general conditions, thereby allowing for typical settings encountered in many econometric applications where the errors may be non-Gaussian, autocorrelated, heteroskedastic and weakly dependent. Finite-sample simulations demonstrate strong performance relative to benchmarks, and empirical applications illustrate StarTime’s usefulness for analyzing financial and macroeconomic data. An R package `StarTime` implementing the proposed method, along with replication code for all results in this paper, is available at [https://github.com/MarieCorillon/StarTime\\_Replication](https://github.com/MarieCorillon/StarTime_Replication).

Several avenues for future research remain. While we focus on  $\ell_1$ -penalization to promote sparsity and temporal aggregation through parameter fusion in  $\beta$ , alternative penalties could explore other structured forms of aggregation and sparsity (e.g., Nicholson et al., 2020; Yan and Bien, 2017). Furthermore, we select tuning parameters via a Bayesian Information Criterion for simplicity; extending data-driven tuning parameter approaches such as Kock et al. (2025) may further narrow the gap to Oracle performance. Extending valid high-dimensional inference procedures developed for sparse time series models (e.g., Adamek et al., 2023) to settings that jointly incorporate temporal aggregation and sparsity represents another promising direction for future research.

**Acknowledgments.** The first and third author are financially supported by a grant from the Dutch Research Council (NWO), research programme Vidi (VI.Vidi.211.032). Previous versions of this paper were presented at NESG 2025 and ICSDS 2025; we gratefully acknowledge comments by the participants. We thank Jacob Bien, Enrico Wegner and Etienne Wijler for helpful discussions.

## References

- Adamek, R.; Smeekes, S. and Wilms, I. (2023), “Lasso inference for high-dimensional time series,” *Journal of Econometrics*, 235, 1114–1143.
- Amburgey, A. J. and McCracken, M. W. (2023), “On the real-time predictive content of financial condition indices for growth,” *Journal of Applied Econometrics*, 38, 137–163.
- Amemiya, T. and Wu, R. Y. (1972), “The effect of aggregation on prediction in the autoregressive model,” *Journal of the American Statistical Association*, 67, 628–632.
- Andersen, T. G.; Bollerslev, T.; Diebold, F. X. and Labys, P. (2003), “Modeling and forecasting realized volatility,” *Econometrica*, 71, 579–625.

- Andreou, E. (2016), “On the use of high frequency measures of volatility in MIDAS regressions,” *Journal of Econometrics*, 193, 367–389.
- Audrino, F. and Knaus, S. D. (2016), “Lassoing the HAR model: A model selection perspective on realized volatility dynamics,” *Econometric Reviews*, 35, 1485–1521.
- Audrino, F.; Sigrist, F. and Ballinari, D. (2020), “The impact of sentiment and attention measures on stock market volatility,” *International Journal of Forecasting*, 36, 334–357.
- Babii, A.; Ghysels, E. and Striaukas, J. (2022), “Machine learning time series regressions with an application to nowcasting,” *Journal of Business & Economic Statistics*, 40, 1094–1106.
- (2024), “High-dimensional Granger causality tests with an application to VIX and news,” *Journal of Financial Econometrics*, 22, 605–635.
- Baker, S. R.; Bloom, N. and Davis, S. J. (2016), “Measuring economic policy uncertainty,” *The Quarterly Journal of Economics*, 131, 1593–1636.
- (2026), “Economic Policy Uncertainty Index,” <https://www.policyuncertainty.com>, accessed: 2026-01-20.
- Bernardi, M. and Catania, L. (2018), “The model confidence set package for R,” *International Journal of Computational Economics and Econometrics*, 8, 144–158.
- Blinder, A. S. and Maccini, L. J. (1991), “The resurgence of inventory research: What have we learned?” *Journal of Economic Surveys*, 5, 291–328.
- Bollerslev, T.; Litvinova, J. and Tauchen, G. (2006), “Leverage and volatility feedback effects in high-frequency data,” *Journal of Financial Econometrics*, 4, 353–384.
- Boyd, S.; Parikh, N.; Chu, E.; Peleato, B. and Eckstein, J. (2011), “Distributed optimization and statistical learning via the alternating direction method of multipliers,” *Foundations and Trends in Machine Learning*, 3, 1–122.
- Brave, S. and Butters, R. A. (2011), “Monitoring financial stability: A financial conditions index approach,” *Economic Perspectives*, 35, 22–43.
- Brewer, K. (1973), “Some consequences of temporal aggregation and systematic sampling for ARMA and ARMAX models,” *Journal of Econometrics*, 1, 133–154.

- Bühlmann, P. and van de Geer, S. (2011), *Statistics for high-dimensional data: Methods, theory and applications*, Springer.
- Chassot, J. and Audrino, F. (2026), “HARd to beat: The overlooked impact of rolling windows in the era of machine learning,” *International Journal of Forecasting*, 42, 330–343.
- Chen, J. and Chen, Z. (2012), “Extended BIC for small- $n$ -large- $P$  sparse GLM,” *Statistica Sinica*, 22, 555–574.
- Cheung, C. and Granovsky, D. (2016), “New housing registrations as a leading indicator of the BC economy,” Tech. Rep. 2016-3, Bank of Canada Staff Discussion Paper.
- Christensen, K.; Siggaard, M. and Veliyev, B. (2023), “A machine learning approach to volatility forecasting,” *Journal of Financial Econometrics*, 21, 1680–1727.
- Corsi, F. (2009), “A simple approximate long-memory model of realized volatility,” *Journal of Financial Econometrics*, 7, 174–196.
- Cortes, G. and LaPoint, C. (2024), “Housing Is the Financial Cycle: Evidence from 100 Years of Local Building Permits,” SSRN Working Paper No. 4855353.
- Diebold, F. X. and Mariano, R. S. (1995), “Comparing predictive accuracy,” *Journal of Business & Economic Statistics*, 13, 253–263.
- Forni, C.; Marcellino, M. and Schumacher, C. (2015), “Unrestricted mixed data sampling (MIDAS): MIDAS regressions with unrestricted lag polynomials,” *Journal of the Royal Statistical Society: Series A (Statistics in Society)*, 178, 57–82.
- Friedman, J.; Hastie, T. and Tibshirani, R. (2010), “Regularization paths for generalized linear models via coordinate descent,” *Journal of Statistical Software*, 33, 1–22.
- Fu, J.; Molstad, A. J. and Zou, H. (2025), “A direct approach to tree-guided feature aggregation for high-dimensional regression,” arXiv preprint 2507.19650.
- Ghysels, E.; Kvedaras, V. and Zemlys, V. (2016), “Mixed frequency data sampling regression models: The R package midasr,” *Journal of Statistical Software*, 72, 1–35.
- Ghysels, E.; Santa-Clara, P. and Valkanov, R. (2004), “The MIDAS touch: Mixed data sampling regression models,” CIRANO Working Paper 2004s-20, CIRANO.

- Ghysels, E.; Sinko, A. and Valkanov, R. (2007), “MIDAS regressions: Further results and new directions,” *Econometric reviews*, 26, 53–90.
- Giannone, D.; Reichlin, L. and Small, D. (2008), “Nowcasting: The real-time informational content of macroeconomic data,” *Journal of Monetary Economics*, 55, 665–676.
- Hansen, P. R.; Lunde, A. and Nason, J. M. (2011), “The model confidence set,” *Econometrica*, 79, 453–497.
- Hastie, T.; Tibshirani, R. and Wainwright, M. (2015), *Statistical learning with sparsity: The lasso and generalizations*, Chapman and Hall/CRC, 1st ed.
- Hecq, A.; Margaritella, L. and Smeekes, S. (2023), “Granger causality testing in high-dimensional VARs: A post-double-selection procedure,” *Journal of Financial Econometrics*, 21, 915–958.
- Hecq, A.; Ternes, M. and Wilms, I. (2022), “Hierarchical regularizers for mixed-frequency vector autoregressions,” *Journal of Computational and Graphical Statistics*, 31, 1076–1090.
- Hoerl, A. E. and Kennard, R. W. (1970), “Ridge regression: Biased estimation for nonorthogonal problems,” *Technometrics*, 12, 55–67.
- Hubert, L. and Arabie, P. (1985), “Comparing partitions,” *Journal of Classification*, 2, 193–218.
- Hyndman, R. J. and Khandakar, Y. (2008), “Automatic time series forecasting: The forecast package for R,” *Journal of Statistical Software*, 27, 1–22.
- Kock, A. B.; Pedersen, R. S. and Sørensen, J. R.-V. (2025), “Data-driven tuning parameter selection for high-dimensional vector autoregressions,” *Journal of the American Statistical Association*, 1–19.
- Leamer, E. E. (2007), “Housing is the business cycle,” NBER Working Paper 13428, National Bureau of Economic Research.
- Luo, Y.; Xue, X. and Izzeldin, M. (2025), “When MIDAS meets LASSO: The power of low-frequency variables in forecasting value-at-risk and expected shortfall,” *Journal of Financial Econometrics*, 23.
- Marcellino, M.; Stock, J. H. and Watson, M. W. (2006), “A comparison of direct and iterated multistep AR methods for forecasting macroeconomic time series,” *Journal of Econometrics*, 135, 499–526.

- Masini, R. P.; Medeiros, M. C. and Mendes, E. F. (2023), “Machine learning advances for time series forecasting,” *Journal of Economic Surveys*, 37, 76–111.
- McCracken, M. W. and Ng, S. (2016), “FRED-MD: A Monthly Database for Macroeconomic Research,” *Journal of Business & Economic Statistics*, 34, 574–589.
- (2021), “FRED-QD: A Quarterly Database for Macroeconomic Research,” *Federal Reserve Bank of St. Louis Review*, 103, 1–44.
- Medeiros, M. C. and Mendes, E. F. (2016), “ $\ell_1$ -regularization of high-dimensional time-series models with non-Gaussian and heteroskedastic errors,” *Journal of Econometrics*, 191, 255–271.
- Mogliani, M. and Simoni, A. (2021), “Bayesian MIDAS penalized regressions: Estimation, selection, and prediction,” *Journal of Econometrics*, 222, 833–860.
- NBER Business Cycle Dating Committee (2025), “Business cycle dating procedure: Frequently asked questions,” National Bureau of Economic Research.
- Nicholson, W. B.; Wilms, I.; Bien, J. and Matteson, D. S. (2020), “High dimensional forecasting via interpretable vector autoregression,” *Journal of Machine Learning Research*, 21, 1–52.
- Patton, A. J. (2011), “Volatility forecast comparison using imperfect volatility proxies,” *Journal of Econometrics*, 160, 246–256, realized Volatility.
- Poon, S.-H. and Granger, C. W. J. (2003), “Forecasting volatility in financial markets: A review,” *Journal of Economic Literature*, 41, 478–539.
- R Core Team (2025), *R: A Language and Environment for Statistical Computing*, R Foundation for Statistical Computing, Vienna, Austria.
- Rossana, R. and Seater, J. (1995), “Temporal aggregation and economic time series,” *Journal of Business & Economic Statistics*, 13, 441–51.
- Schumacher, C. (2016), “A comparison of MIDAS and bridge equations,” *International Journal of Forecasting*, 32, 257–270.
- Smeekes, S. and Wijler, E. (2021), “An automated approach towards sparse single-equation cointegration modelling,” *Journal of Econometrics*, 221, 247–276.
- Smeekes, S. and Wilms, I. (2023), “bootUR: An R package for bootstrap unit root tests,” *Journal of Statistical Software*, 106, 1–39.

- Stock, J. H. and Watson, M. W. (1989), “New indexes of coincident and leading economic indicators,” in *NBER Macroeconomics Annual 1989, Volume 4*, MIT Press, pp. 351–394.
- (2007), “Why has U.S. inflation become harder to forecast?” *Journal of Money, Credit and Banking*, 39, 3–33.
- Striaukas, J.; Babii, A. and Ghysels, E. (2022), *midasml: Estimation and prediction methods for high-dimensional mixed frequency time series data*, R package version 0.1.10.
- Taylor, N. (2019), “Forecasting returns in the VIX futures market,” *International Journal of Forecasting*, 35, 1193–1210.
- Tiao, G. C. (1972), “Asymptotic behaviour of temporal aggregates of time series,” *Biometrika*, 59, 525–531.
- Tibshirani, R. (1996), “Regression shrinkage and selection via the lasso,” *Journal of the Royal Statistical Society. Series B (Methodological)*, 58, 267–288.
- Todorov, V. and Tauchen, G. (2012), “The realized Laplace transform of volatility,” *Econometrica*, 80, 1105–1127.
- Veredas, D. and Silvestrini, A. (2008), “Temporal aggregation of univariate and multivariate time series models: A survey,” *Journal of Economic Surveys*, 22, 458–497.
- Wilms, I. and Bien, J. (2022), “Tree-based node aggregation in sparse graphical models,” *Journal of Machine Learning Research*, 23, 1–36.
- Yan, X. and Bien, J. (2017), “Hierarchical sparse modeling: A choice of two group lasso formulations,” *Statistical Science*, 32, 531–560.
- (2021), “Rare feature selection in high dimensions,” *Journal of the American Statistical Association*, 116, 887–900.
- Zarnowitz, V. (1992), *Business cycles: Theory, history, indicators, and forecasting*, University of Chicago Press.
- Zhang, C.; Zhang, Y.; Cucuringu, M. and Qian, Z. (2024), “Volatility forecasting with machine learning and intraday commonality,” *Journal of Financial Econometrics*, 22, 492–530.
- Zou, H. and Hastie, T. (2005), “Regularization and variable selection via the elastic net,” *Journal of the Royal Statistical Society Series B: Statistical Methodology*, 67, 301–320.

## A Theory

### A.1 Preliminary Results

**Lemma 1** (Basic Inequality). *We have*

$$\frac{1}{2T} \left\| \mathbf{X}(\hat{\boldsymbol{\beta}} - \boldsymbol{\beta}^0) \right\|_2^2 + \lambda \|w(\hat{\boldsymbol{\gamma}})\|_1 \leq \frac{\boldsymbol{\varepsilon}^\top \mathbf{X}(\hat{\boldsymbol{\beta}} - \boldsymbol{\beta}^0)}{T} + \lambda \|w(\boldsymbol{\gamma}^0)\|_1.$$

*Proof of Lemma 1.* Using  $\mathbf{y} = \mathbf{X}\boldsymbol{\beta}^0 + \boldsymbol{\varepsilon}$ , we have

$$\begin{aligned} & \frac{1}{2T} \left\| \mathbf{y} - \mathbf{X}\hat{\boldsymbol{\beta}} \right\|_2^2 + \lambda \|w(\hat{\boldsymbol{\gamma}})\|_1 \leq \frac{1}{2T} \left\| \mathbf{y} - \mathbf{X}\boldsymbol{\beta}^0 \right\|_2^2 + \lambda \|w(\boldsymbol{\gamma}^0)\|_1 \\ \iff & \frac{1}{2T} \left\| \mathbf{X}\boldsymbol{\beta}^0 + \boldsymbol{\varepsilon} - \mathbf{X}\hat{\boldsymbol{\beta}} \right\|_2^2 + \lambda \|w(\hat{\boldsymbol{\gamma}})\|_1 \leq \frac{1}{2T} \left\| \mathbf{X}\boldsymbol{\beta}^0 + \boldsymbol{\varepsilon} - \mathbf{X}\boldsymbol{\beta}^0 \right\|_2^2 + \lambda \|w(\boldsymbol{\gamma}^0)\|_1 \\ \iff & \frac{1}{2T} \left( \|\boldsymbol{\varepsilon}\|_2^2 + 2\boldsymbol{\varepsilon}^\top \mathbf{X}(\hat{\boldsymbol{\beta}} - \boldsymbol{\beta}^0) + \left\| \mathbf{X}(\hat{\boldsymbol{\beta}} - \boldsymbol{\beta}^0) \right\|_2^2 \right) + \lambda \|w(\hat{\boldsymbol{\gamma}})\|_1 \leq \frac{1}{2T} \|\boldsymbol{\varepsilon}\|_2^2 + \lambda \|w(\boldsymbol{\gamma}^0)\|_1 \\ \iff & \frac{1}{2T} \left\| \mathbf{X}(\hat{\boldsymbol{\beta}} - \boldsymbol{\beta}^0) \right\|_2^2 + \lambda \|w(\hat{\boldsymbol{\gamma}})\|_1 \leq \frac{\boldsymbol{\varepsilon}^\top \mathbf{X}(\hat{\boldsymbol{\beta}} - \boldsymbol{\beta}^0)}{T} + \lambda \|w(\boldsymbol{\gamma}^0)\|_1 \end{aligned}$$

□

**Lemma 2** (Concentration). *Let Assumption 1 be satisfied and recall  $\mathcal{J} = \left\{ \frac{\|\mathbf{X}^\top \boldsymbol{\varepsilon}\|_\infty}{T} \leq \lambda_0 \right\}$ . Then, for  $\lambda_0 := C \frac{N^{1/\tilde{m}}(\ln \ln T)^{1/\tilde{m}}}{\sqrt{T}}$ ,*

$$\mathbb{P}(\mathcal{J}) \geq 1 - C(\ln \ln T)^{-1}.$$

*Proof of Lemma 2.* Let  $V_j := \sum_{t=1}^T x_{j,t} \varepsilon_t$  and  $C_1 > 0$ . Then, the complement of  $\mathcal{J}$ ,  $\mathcal{J}^c$ , can be expressed as

$$\mathbb{P}(\mathcal{J}^c) = \mathbb{P}\left( \max_{1 \leq j \leq N} |V_j| > T\lambda_0 \right) \leq C_1 N \left( \frac{1}{\lambda_0 \sqrt{T}} \right)^{\tilde{m}},$$

where the inequality follows from [Adamek et al. \(2023\)](#)'s Lemma A.4. Let  $L_T \rightarrow \infty$  as  $T \rightarrow \infty$  be any deterministic sequence and choose

$$\lambda_0 := C_2 \frac{N^{1/\tilde{m}} L_T^{1/\tilde{m}}}{\sqrt{T}},$$

for some  $C_2 > 0$ . Then

$$\mathbb{P}(\mathcal{J}^c) \leq C_1 N \left( \frac{1}{C_2 N^{1/\tilde{m}} L_T^{1/\tilde{m}}} \right)^{\tilde{m}} = \frac{C}{L_T},$$

and

$$\mathbb{P}(\mathcal{J}) \geq 1 - \frac{C}{L_T}.$$

In particular, for  $L_T = \ln \ln T$ , we obtain  $\mathbb{P}(\mathcal{J}) \geq 1 - C(\ln \ln T)^{-1} \rightarrow 1$  as  $T \rightarrow \infty$ .  $\square$

**Lemma 3** (Initial Error Bound). *Under Assumption 1 and for  $C > 0$ , let the tuning parameter be*

$$\lambda := 2C \frac{N^{1/\tilde{m}} (\ln \ln T)^{1/\tilde{m}}}{\sqrt{T}}.$$

With probability at least  $1 - \frac{C}{\ln \ln T}$ , we have

$$\frac{1}{2T} \left\| \mathbf{X}(\hat{\boldsymbol{\beta}} - \boldsymbol{\beta}^0) \right\|_2^2 \leq \frac{3}{2} \lambda \|w(\boldsymbol{\gamma}^0)\|_1.$$

*Proof of Lemma 3.* On the event

$$\mathcal{J} := \left\{ \frac{\|\mathbf{X}^\top \boldsymbol{\varepsilon}\|_\infty}{T} \leq \lambda_0 \right\},$$

Lemma 1 yields

$$\frac{1}{2T} \left\| \mathbf{X}(\hat{\boldsymbol{\beta}} - \boldsymbol{\beta}^0) \right\|_2^2 + \lambda \|w(\hat{\boldsymbol{\gamma}})\|_1 \leq \frac{\boldsymbol{\varepsilon}^\top \mathbf{X}(\hat{\boldsymbol{\beta}} - \boldsymbol{\beta}^0)}{T} + \lambda \|w(\boldsymbol{\gamma}^0)\|_1.$$

Using Hölder's inequality and the definition of  $\mathcal{J}$ , we have

$$\left| \frac{\boldsymbol{\varepsilon}^\top \mathbf{X}(\hat{\boldsymbol{\beta}} - \boldsymbol{\beta}^0)}{T} \right| = \left| \frac{(\mathbf{X}^\top \boldsymbol{\varepsilon})^\top (\hat{\boldsymbol{\beta}} - \boldsymbol{\beta}^0)}{T} \right| \leq \frac{\|\mathbf{X}^\top \boldsymbol{\varepsilon}\|_\infty}{T} \|\hat{\boldsymbol{\beta}} - \boldsymbol{\beta}^0\|_1 \leq \lambda_0 \|\hat{\boldsymbol{\beta}} - \boldsymbol{\beta}^0\|_1.$$

Assume now that  $\lambda \geq 2\lambda_0$ , then

$$\frac{\boldsymbol{\varepsilon}^\top \mathbf{X}(\hat{\boldsymbol{\beta}} - \boldsymbol{\beta}^0)}{T} \leq \left| \frac{\boldsymbol{\varepsilon}^\top \mathbf{X}(\hat{\boldsymbol{\beta}} - \boldsymbol{\beta}^0)}{T} \right| \leq \frac{\lambda}{2} \|\hat{\boldsymbol{\beta}} - \boldsymbol{\beta}^0\|_1.$$

Substituting this bound into the basic inequality gives

$$\frac{1}{2T} \left\| \mathbf{X}(\hat{\boldsymbol{\beta}} - \boldsymbol{\beta}^0) \right\|_2^2 + \lambda \|w(\hat{\boldsymbol{\gamma}})\|_1 \leq \frac{\lambda}{2} \|\hat{\boldsymbol{\beta}} - \boldsymbol{\beta}^0\|_1 + \lambda \|w(\boldsymbol{\gamma}^0)\|_1.$$

Finally, using  $\|\hat{\boldsymbol{\beta}} - \boldsymbol{\beta}^0\|_1 \leq \|w(\hat{\boldsymbol{\gamma}}) - w(\boldsymbol{\gamma}^0)\|_1$  and the triangle inequality

$$\|w(\hat{\boldsymbol{\gamma}}) - w(\boldsymbol{\gamma}^0)\|_1 \leq \|w(\hat{\boldsymbol{\gamma}})\|_1 + \|w(\boldsymbol{\gamma}^0)\|_1,$$

we obtain

$$\begin{aligned} \frac{1}{2T} \left\| \mathbf{X}(\hat{\boldsymbol{\beta}} - \boldsymbol{\beta}^0) \right\|_2^2 + \lambda \|w(\hat{\boldsymbol{\gamma}})\|_1 &\leq \frac{\lambda}{2} \left( \|w(\hat{\boldsymbol{\gamma}})\|_1 + \|w(\boldsymbol{\gamma}^0)\|_1 \right) + \lambda \|w(\boldsymbol{\gamma}^0)\|_1 \\ &= \frac{\lambda}{2} \|w(\hat{\boldsymbol{\gamma}})\|_1 + \frac{3\lambda}{2} \|w(\boldsymbol{\gamma}^0)\|_1. \end{aligned}$$

Subtract  $\frac{\lambda}{2} \|w(\hat{\boldsymbol{\gamma}})\|_1$  from both sides to obtain

$$\frac{1}{2T} \left\| \mathbf{X}(\hat{\boldsymbol{\beta}} - \boldsymbol{\beta}^0) \right\|_2^2 + \frac{\lambda}{2} \|w(\hat{\boldsymbol{\gamma}})\|_1 \leq \frac{3\lambda}{2} \|w(\boldsymbol{\gamma}^0)\|_1.$$

Since  $\frac{\lambda}{2} \|w(\hat{\boldsymbol{\gamma}})\|_1 \geq 0$ , we can drop this non-negative term from the left-hand side, yielding

$$\frac{1}{2T} \left\| \mathbf{X}(\hat{\boldsymbol{\beta}} - \boldsymbol{\beta}^0) \right\|_2^2 \leq \frac{3\lambda}{2} \|w(\boldsymbol{\gamma}^0)\|_1.$$

The associated probability stems from Lemma 2. □

**Lemma 4** (Cone Decomposition). *On the event  $\mathcal{J}$  of Lemma 2 and under the conditions of Lemma 1 and Lemma 3, the StarTime estimator  $\hat{\boldsymbol{\beta}}$  satisfies*

$$\frac{1}{T} \left\| \mathbf{X}(\hat{\boldsymbol{\beta}} - \boldsymbol{\beta}^0) \right\|_2^2 + \lambda \|w(\hat{\boldsymbol{\gamma}})_{S_0^c}\|_1 \leq 3\lambda \|w(\hat{\boldsymbol{\gamma}})_{S_0} - w(\boldsymbol{\gamma}^0)_{S_0}\|_1.$$

*Proof of Lemma 4.* Starting from Lemma 1 multiplied by a factor of 2, we have

$$\frac{1}{T} \left\| \mathbf{X}(\hat{\boldsymbol{\beta}} - \boldsymbol{\beta}^0) \right\|_2^2 + 2\lambda \|w(\hat{\boldsymbol{\gamma}})\|_1 \leq \frac{2}{T} \boldsymbol{\varepsilon}^\top \mathbf{X}(\hat{\boldsymbol{\beta}} - \boldsymbol{\beta}^0) + 2\lambda \|w(\boldsymbol{\gamma}^0)\|_1. \quad (15)$$

On the event  $\mathcal{J}$ , the empirical-process bound gives

$$\frac{1}{T} \left| \boldsymbol{\varepsilon}^\top \mathbf{X}(\hat{\boldsymbol{\beta}} - \boldsymbol{\beta}^0) \right| \leq \lambda_0 \left\| \hat{\boldsymbol{\beta}} - \boldsymbol{\beta}^0 \right\|_1.$$

Substituting this bound into (15) and using  $\lambda \geq 2\lambda_0$  yields

$$\frac{1}{T} \left\| \mathbf{X}(\hat{\boldsymbol{\beta}} - \boldsymbol{\beta}^0) \right\|_2^2 + 2\lambda \|w(\hat{\boldsymbol{\gamma}})\|_1 \leq \lambda \left\| \hat{\boldsymbol{\beta}} - \boldsymbol{\beta}^0 \right\|_1 + 2\lambda \|w(\boldsymbol{\gamma}^0)\|_1. \quad (16)$$

Since  $w(\boldsymbol{\gamma}^0)_{S_0^c} = \mathbf{0}$ , we can write

$$\|w(\hat{\boldsymbol{\gamma}})\|_1 = \|w(\hat{\boldsymbol{\gamma}})_{S_0}\|_1 + \|w(\hat{\boldsymbol{\gamma}})_{S_0^c}\|_1, \quad \|w(\boldsymbol{\gamma}^0)\|_1 = \|w(\boldsymbol{\gamma}^0)_{S_0}\|_1.$$

We first focus on the penalty term on the left-hand side of (16). Using the triangle inequality in the form  $\|a\|_1 \geq \|b\|_1 - \|a - b\|_1$ , we have

$$\begin{aligned} \|w(\hat{\gamma})_{S_0}\|_1 &= \left\| w(\gamma^0)_{S_0} + \left( w(\hat{\gamma})_{S_0} - w(\gamma^0)_{S_0} \right) \right\|_1 \\ &\geq \|w(\gamma^0)_{S_0}\|_1 - \|w(\hat{\gamma})_{S_0} - w(\gamma^0)_{S_0}\|_1. \end{aligned}$$

Substituting this lower bound into the left-hand side of (16) gives

$$\begin{aligned} &\frac{1}{T} \left\| \mathbf{X}(\hat{\beta} - \beta^0) \right\|_2^2 + 2\lambda \|w(\hat{\gamma})_{S_0}\|_1 + 2\lambda \|w(\hat{\gamma})_{S_0^c}\|_1 \\ &\geq \frac{1}{T} \left\| \mathbf{X}(\hat{\beta} - \beta^0) \right\|_2^2 + 2\lambda \|w(\gamma^0)_{S_0}\|_1 - 2\lambda \|w(\hat{\gamma})_{S_0} - w(\gamma^0)_{S_0}\|_1 + 2\lambda \|w(\hat{\gamma})_{S_0^c}\|_1. \end{aligned}$$

Now we turn to the term  $\left\| \hat{\beta} - \beta^0 \right\|_1$  on the right-hand side of (16). We use that

$$\begin{aligned} \left\| \hat{\beta} - \beta^0 \right\|_1 &\leq \|\hat{\gamma} - \gamma^0\|_1 + \|\mathbf{A}(\hat{\gamma} - \gamma^0)\|_1 \\ &= \|w(\hat{\gamma}) - w(\gamma^0)\|_1 \\ &= \|w(\hat{\gamma})_{S_0} - w(\gamma^0)_{S_0}\|_1 + \|w(\hat{\gamma})_{S_0^c}\|_1. \end{aligned}$$

Therefore, the right-hand side of (16) is bounded above by

$$\lambda \|w(\hat{\gamma})_{S_0} - w(\gamma^0)_{S_0}\|_1 + \lambda \|w(\hat{\gamma})_{S_0^c}\|_1 + 2\lambda \|w(\gamma^0)_{S_0}\|_1.$$

Combining the preceding two displays with (16) and rearranging terms yields

$$\frac{1}{T} \left\| \mathbf{X}(\hat{\beta} - \beta^0) \right\|_2^2 + \lambda \|w(\hat{\gamma})_{S_0^c}\|_1 \leq 3\lambda \|w(\hat{\gamma})_{S_0} - w(\gamma^0)_{S_0}\|_1.$$

□

**Lemma 5** (Active Set Bounding). *Under Assumption 2 and for every  $\gamma$  on the cone, that is,  $\left\{ \gamma \in \mathbb{R}^M : \|w(\gamma)_{S_0^c}\|_1 \leq 3\|w(\gamma)_{S_0}\|_1 \right\}$ , we have*

$$\|\beta\|_1 \leq \|w(\gamma)\|_1 \leq 4\|w(\gamma)_{S_0}\|_1. \quad (17)$$

*Proof of Lemma 5.* On the cone,

$$\|w(\gamma)\|_1 = \|w(\gamma)_{S_0^c}\|_1 + \|w(\gamma)_{S_0}\|_1 \leq 4\|w(\gamma)_{S_0}\|_1.$$

The initial cone condition is a direct result from Lemma 4.  $\square$

**Lemma 6** (Sample Compatibility). *For every  $\gamma$  on the cone, that is,  $\{\gamma \in \mathbb{R}^M : \|w(\gamma)_{S_0^c}\|_1 \leq 3\|w(\gamma)_{S_0}\|_1\}$ , and under Assumptions 1, 2 and 3, we have the following sample compatibility condition on the set  $\mathcal{C}(S_0) := \left\{ \left\| \hat{\Sigma} - \Sigma \right\|_\infty \leq C/s_0 \right\}$ ,*

$$s_0 \beta^\top \hat{\Sigma} \beta \geq \rho_0^2 \|w(\gamma)_{S_0}\|_1^2,$$

where  $\rho_0 > 0$ .

*Proof of Lemma 6.* Let  $\gamma \in \mathbb{R}^M$  satisfy  $\|w(\gamma)_{S_0^c}\|_1 \leq 3\|w(\gamma)_{S_0}\|_1$ . Observe that, on the set  $\mathcal{C}(S_0) := \left\{ \left\| \hat{\Sigma} - \Sigma \right\|_\infty \leq C/s_0 \right\}$  and using Lemma 5 for the third inequality,

$$\begin{aligned} \left| \beta^\top (\hat{\Sigma} - \Sigma) \beta \right| &\leq \left\| \hat{\Sigma} - \Sigma \right\|_\infty \|\beta\|_1^2 \leq \frac{C}{s_0} \|\beta\|_1^2 \leq \frac{C}{s_0} \|w(\gamma)\|_1^2 \\ &\leq \frac{16C}{s_0} \|w(\gamma)_{S_0}\|_1^2. \end{aligned}$$

So, on  $\mathcal{C}(S_0)$ , we have  $\beta^\top (\hat{\Sigma} - \Sigma) \beta \geq -\frac{16C}{s_0} \|w(\gamma)_{S_0}\|_1^2$ . Then, under Assumption 3,

$$\begin{aligned} s_0 \beta^\top \hat{\Sigma} \beta &= s_0 \beta^\top \Sigma \beta + s_0 \beta^\top (\hat{\Sigma} - \Sigma) \beta \\ &\geq \rho_\Sigma^2 \|w(\gamma)_{S_0}\|_1^2 - 16C \|w(\gamma)_{S_0}\|_1^2 \\ &= \left( \rho_\Sigma^2 - 16C \right) \|w(\gamma)_{S_0}\|_1^2 \end{aligned}$$

with  $\frac{\rho_\Sigma^2}{2} \geq 16C$ , so  $\left( \rho_\Sigma^2 - 16C \right) \geq \frac{\rho_\Sigma^2}{2}$ . Taking  $\rho_0^2 = \frac{\rho_\Sigma^2}{2}$  leads to the sample compatibility condition

$$s_0 \beta^\top \hat{\Sigma} \beta \geq \rho_0^2 \|w(\gamma)_{S_0}\|_1^2. \quad (18)$$

Using Lemma A.3. in Adamek et al. (2023) for the exact sparsity case ( $r = 0$ ), we have that for a sequence  $\eta_T \rightarrow 0$  with  $\eta_T \leq \frac{N^2}{e}$ , and such that  $s_0 \leq C \eta_T^{\frac{d+\tilde{m}-1}{d\tilde{m}+\tilde{m}-1}} \left[ \frac{\sqrt{T}}{N^{\frac{2}{d}+\frac{\tilde{m}}{\tilde{m}-1}}} \right]^{\frac{1}{d}+\frac{\tilde{m}}{\tilde{m}-1}}$ , then  $\mathbb{P}(\mathcal{C}(S_0)) \geq 1 - \eta_T \rightarrow 1$  as  $N, T \rightarrow \infty$ . Hence, the bound in (18) holds with the same probability.  $\square$

## A.2 Proofs of the Main Results

*Proof of Theorem 1.* On the events  $\mathcal{J}$  and  $\mathcal{C}(S_0)$ , and for  $\lambda \geq 2\lambda_0$ , we have

$$\begin{aligned}
\frac{2}{2T} \left\| \mathbf{X}(\hat{\beta} - \beta^0) \right\|_2^2 + \lambda \|w(\hat{\gamma} - \gamma^0)\|_1 &= \frac{2}{2T} \left\| \mathbf{X}(\hat{\beta} - \beta^0) \right\|_2^2 + \lambda \left\| (w(\hat{\gamma}) - w(\gamma^0))_{S_0} \right\|_1 \\
&\quad + \lambda \|w(\hat{\gamma})_{S_0^c}\|_1 \\
&\leq 3\lambda \left\| (w(\hat{\gamma}) - w(\gamma^0))_{S_0} \right\|_1 + \lambda \left\| (w(\hat{\gamma}) - w(\gamma^0))_{S_0} \right\|_1 \\
&\leq 4\lambda \frac{\sqrt{s_0}}{\rho_0} \frac{\left\| \mathbf{X}(\hat{\beta} - \beta^0) \right\|_2}{\sqrt{T}} \\
&\leq \frac{\left\| \mathbf{X}(\hat{\beta} - \beta^0) \right\|_2^2}{2T} + \frac{8\lambda^2 s_0}{\rho_0^2}.
\end{aligned}$$

The first inequality uses Lemma 4, the second inequality uses Lemma 6, and the last inequality uses the identity  $4uv \leq u^2 + 4v^2$ . Subtracting  $\frac{1}{2T} \left\| \mathbf{X}(\hat{\beta} - \beta^0) \right\|_2^2$  from both sides yields

$$\frac{1}{2T} \left\| \mathbf{X}(\hat{\beta} - \beta^0) \right\|_2^2 + \lambda \|w(\hat{\gamma} - \gamma^0)\|_1 \leq \frac{8\lambda^2 s_0}{\rho_0^2}.$$

From Lemma 2, we know that  $\mathcal{J} \geq 1 - C(\ln \ln T)^{-1}$  for  $\lambda := 2C \frac{N^{1/\tilde{m}} (\ln \ln T)^{1/\tilde{m}}}{\sqrt{T}}$ . From Lemma 6, we have that  $\mathbb{P}(\mathcal{C}(S_0)) \geq 1 - \eta_T \rightarrow 1$  for  $\eta_T \leq \frac{N^2}{e}$  and if  $s_0 \leq C\eta_T^{\frac{d+\tilde{m}-1}{d\tilde{m}+\tilde{m}-1}} \left[ \frac{\sqrt{T}}{N^{\frac{2}{d}+\frac{2}{m-1}}} \right]^{\frac{1}{\frac{1}{d}+\frac{\tilde{m}}{m-1}}}$  as  $N, T \rightarrow \infty$ . Choosing  $\eta_T = \ln \ln T$  satisfies those conditions. Hence,  $\mathbb{P}(\mathcal{J} \cap \mathcal{C}(S_0)) = 1 - (1 - \mathbb{P}(\mathcal{J}) - (1 - \mathbb{P}(\mathcal{C}(S_0)))) \geq 1 - C_1(\ln \ln T)^{-1} - C_2(\ln \ln T)^{-1} = 1 - C(\ln \ln T)^{-1}$ .  $\square$

*Proof of Corollary 1.* It follows from Theorem 1 that if  $\frac{1}{2T} \left\| \mathbf{X}(\hat{\beta} - \beta^0) \right\|_2^2 + \lambda \|w(\hat{\gamma} - \gamma^0)\|_1 \leq \frac{8\lambda^2 s_0}{\rho_0^2}$ , then each component on the left-hand side of the inequality is smaller than  $8\lambda^2 s_0 / \rho_0^2$ , with at least the same probability.  $\square$

## B Financial Variables

Table 2: Overview of the 30 Major U.S. Financial Assets

Ticker	Company Name
AAPL	Apple Inc.
AXP	American Express Company
BA	The Boeing Company
CAT	Caterpillar Inc.
CSCO	Cisco Systems, Inc.
CVX	Chevron Corporation
DD	DuPont de Nemours, Inc.
DIS	The Walt Disney Company
GE	General Electric Company
GS	The Goldman Sachs Group, Inc.
HD	The Home Depot, Inc.
IBM	International Business Machines Corporation
INTC	Intel Corporation
JNJ	Johnson & Johnson
JPM	JPMorgan Chase & Co.
KO	The Coca-Cola Company
MCD	McDonald's Corporation
MMM	3M Company
MRK	Merck & Co., Inc.
MSFT	Microsoft Corporation
NKE	NIKE, Inc.
PFE	Pfizer Inc.
PG	The Procter & Gamble Company
TRV	The Travelers Companies, Inc.
UNH	UnitedHealth Group Incorporated
UTX	United Technologies Corporation
V	Visa Inc.
VZ	Verizon Communications Inc.
WMT	Walmart Inc.
XOM	Exxon Mobil Corporation

## C Financial Results

Table 3: Model Confidence Set Inclusion Rates (MSFE)

Configuration			Models				
Lags	Window	Horizon	Random Walk	AR1	HAR	Post StarTime	Simple StarTime
20	125	1	0.000	0.000	1.000	0.000	0.000
20	125	5	0.000	0.633	1.000	0.700	0.767
20	125	20	0.000	1.000	0.667	0.567	0.867
20	250	1	0.000	0.000	1.000	0.067	0.000
20	250	5	0.000	0.033	1.000	0.433	0.433
20	250	20	0.000	0.967	0.967	0.900	0.967
20	1000	1	0.000	0.000	1.000	0.567	0.433
20	1000	5	0.000	0.000	1.000	0.633	0.867
20	1000	20	0.000	0.333	1.000	0.967	1.000
40	125	1	0.000	0.000	1.000	0.000	0.000
40	125	5	0.000	0.400	1.000	0.033	0.367
40	125	20	0.000	1.000	0.800	0.067	0.700
40	250	1	0.000	0.000	1.000	0.067	0.000
40	250	5	0.000	0.033	1.000	0.133	0.067
40	250	20	0.000	0.900	1.000	0.533	0.767
40	1000	1	0.000	0.000	1.000	0.567	0.500
40	1000	5	0.000	0.000	1.000	0.733	0.833
40	1000	20	0.000	0.267	0.967	0.767	0.900

*Note:* Values represent the proportion of stocks included in the 95% MCS.

Table 4: Diebold-Mariano Win / Loss Rates: Post StarTime vs Benchmarks (MSFE)

Configuration			Models			
Lags	Window	Horizon	Random Walk	AR1	HAR	Simple StarTime
20	125	1	1.000 / 0.000	0.933 / 0.000	0.000 / 1.000	0.900 / 0.000
20	125	5	1.000 / 0.000	0.100 / 0.000	0.000 / 0.333	0.033 / 0.033
20	125	20	0.967 / 0.000	0.000 / 0.367	0.000 / 0.033	0.000 / 0.367
20	250	1	1.000 / 0.000	1.000 / 0.000	0.000 / 0.900	0.167 / 0.000
20	250	5	1.000 / 0.000	0.933 / 0.000	0.000 / 0.667	0.000 / 0.000
20	250	20	1.000 / 0.000	0.033 / 0.000	0.000 / 0.067	0.000 / 0.000
20	1000	1	1.000 / 0.000	1.000 / 0.000	0.000 / 0.367	0.067 / 0.000
20	1000	5	1.000 / 0.000	1.000 / 0.000	0.000 / 0.400	0.000 / 0.067
20	1000	20	1.000 / 0.000	0.700 / 0.000	0.000 / 0.100	0.000 / 0.033
40	125	1	1.000 / 0.000	0.800 / 0.000	0.000 / 1.000	0.967 / 0.000
40	125	5	1.000 / 0.000	0.000 / 0.100	0.000 / 1.000	0.000 / 0.267
40	125	20	0.900 / 0.000	0.000 / 0.833	0.000 / 0.767	0.000 / 0.867
40	250	1	1.000 / 0.000	1.000 / 0.000	0.000 / 0.900	0.567 / 0.000
40	250	5	1.000 / 0.000	0.500 / 0.000	0.000 / 0.900	0.000 / 0.000
40	250	20	1.000 / 0.000	0.000 / 0.133	0.000 / 0.600	0.000 / 0.033
40	1000	1	1.000 / 0.000	1.000 / 0.000	0.000 / 0.367	0.233 / 0.000
40	1000	5	1.000 / 0.000	0.967 / 0.000	0.000 / 0.267	0.000 / 0.033
40	1000	20	1.000 / 0.000	0.633 / 0.000	0.000 / 0.167	0.000 / 0.033

*Note:* Win Rate / Loss Rate. Win = Post StarTime performs significantly better; Loss = Post StarTime performs significantly worse.

Table 5: Model Confidence Set Inclusion Rates (QLIKE)

Configuration			Models				
Lags	Window	Horizon	Random Walk	AR1	HAR	Post StarTime	Simple StarTime
20	125	1	0.133	0.633	1.000	0.467	0.300
20	125	5	0.167	0.967	1.000	0.867	0.967
20	125	20	0.100	1.000	0.667	0.633	0.867
20	250	1	0.067	0.700	1.000	0.800	0.667
20	250	5	0.067	0.933	1.000	0.967	0.967
20	250	20	0.067	1.000	0.967	0.933	1.000
20	1000	1	0.067	0.933	0.967	0.967	0.800
20	1000	5	0.033	0.933	1.000	0.967	1.000
20	1000	20	0.033	1.000	0.900	0.867	0.967
40	125	1	0.133	0.667	1.000	0.433	0.267
40	125	5	0.133	1.000	1.000	0.600	0.867
40	125	20	0.033	1.000	0.733	0.267	0.767
40	250	1	0.067	0.700	1.000	0.800	0.600
40	250	5	0.067	0.933	1.000	0.833	0.867
40	250	20	0.067	1.000	0.867	0.767	0.867
40	1000	1	0.100	0.933	0.967	0.900	0.767
40	1000	5	0.067	0.900	1.000	0.967	0.967
40	1000	20	0.000	1.000	1.000	0.800	0.967

*Note:* Values represent the proportion of stocks included in the 95% MCS.

Table 6: Diebold-Mariano Win / Loss Rates: Post StarTime vs Benchmarks (QLIKE)

Configuration			Models			
Lags	Window	Horizon	Random Walk	AR1	HAR	Simple StarTime
20	125	1	0.800 / 0.000	0.067 / 0.033	0.000 / 0.533	0.467 / 0.000
20	125	5	0.900 / 0.000	0.000 / 0.067	0.000 / 0.167	0.000 / 0.067
20	125	20	0.633 / 0.000	0.000 / 0.333	0.000 / 0.033	0.000 / 0.300
20	250	1	0.900 / 0.000	0.333 / 0.000	0.000 / 0.300	0.233 / 0.000
20	250	5	0.933 / 0.000	0.067 / 0.000	0.000 / 0.167	0.000 / 0.000
20	250	20	0.967 / 0.000	0.000 / 0.033	0.000 / 0.067	0.000 / 0.167
20	1000	1	0.833 / 0.000	0.067 / 0.033	0.000 / 0.000	0.133 / 0.000
20	1000	5	0.967 / 0.000	0.100 / 0.000	0.000 / 0.067	0.000 / 0.000
20	1000	20	1.000 / 0.000	0.000 / 0.000	0.000 / 0.033	0.000 / 0.167
40	125	1	0.833 / 0.000	0.033 / 0.033	0.000 / 0.600	0.433 / 0.000
40	125	5	0.733 / 0.000	0.000 / 0.300	0.000 / 0.467	0.000 / 0.200
40	125	20	0.633 / 0.000	0.000 / 0.600	0.000 / 0.300	0.000 / 0.700
40	250	1	0.867 / 0.000	0.300 / 0.000	0.000 / 0.233	0.433 / 0.000
40	250	5	0.900 / 0.000	0.033 / 0.033	0.000 / 0.333	0.000 / 0.000
40	250	20	0.933 / 0.000	0.000 / 0.233	0.000 / 0.067	0.000 / 0.167
40	1000	1	0.767 / 0.000	0.067 / 0.033	0.000 / 0.067	0.233 / 0.000
40	1000	5	0.967 / 0.000	0.100 / 0.000	0.000 / 0.000	0.000 / 0.000
40	1000	20	1.000 / 0.000	0.000 / 0.033	0.000 / 0.067	0.000 / 0.133

*Note:* Win Rate / Loss Rate. Win = Post StarTime performs significantly better; Loss = Post StarTime performs significantly worse.

## D Macroeconomic Variables

Table 7: Daily Macroeconomic Data Series

Series Name	Code	Transformation
<i>Market Indices</i>		
S&P 500	SP500	$\Delta \log(x)$
Dow Jones Industrial Average	DJIA	$\Delta \log(x)$
NASDAQ Composite Index	NASDAQCOM	$\Delta \log(x)$
CBOE Volatility Index: VIX	VIXCLS	$\log(x)$
<i>Policy Uncertainty</i>		
Economic Policy Uncertainty	EPU	$\log(x)$

*Note: None of the daily macroeconomic data series are seasonally adjusted, nor are any included in the reduced set.*

Table 8: Weekly Macroeconomic Data Series

Series Name	Code	Transformation	Reduced Set
<i>Financial Indicators</i>			
Chicago Fed National Financial Conditions Index	NFCI	$x$	✓
<i>Labor Market</i>			
Continued Claims (Insured Unemployment)*	CCSA	$\Delta \log(x)$	
Initial Claims*	ICSA	$\Delta \log(x)$	✓

*Note: Series marked with an asterisk (\*) are seasonally adjusted. A checkmark (✓) indicates the variable is included in the reduced set.*

Table 9: Monthly Macroeconomic Data Series

Series Name	Code	Transformation	Reduced Set
<i>Income, Consumption, and Retail</i>			
Real Personal Income*	RPI	$\Delta \log(x)$	
Real Disposable Personal Income*	DSPIC96	$\Delta \log(x)$	
Advance Retail Sales*	RSAFS	$\Delta \log(x)$	✓
Real Manufacturing and Trade Industries Sales*	CMRMTSPL	$\Delta \log(x)$	
<i>Labor Market</i>			
Unemployment Rate*	UNRATE	$\Delta x$	✓
All Employees, Total Nonfarm*	PAYEMS	$\Delta \log(x)$	✓
<i>Real Economic Activity</i>			
Industrial Production: Total Index*	INDPRO	$\Delta \log(x)$	✓
Capacity Utilization: Total Index*	TCU	$\Delta x$	
Total Business Inventories*	BUSINV	$\Delta \log(x)$	
Manufacturers' New Orders: Total Manufacturing*	AMTMNO	$\Delta \log(x)$	✓
New Privately-Owned Housing Units Started*	HOUST	$\log(x)$	✓
New Privately-Owned Housing Units Authorized*	PERMIT	$\log(x)$	✓
New One Family Houses Sold*	HSN1F	$\log(x)$	
<i>Prices and Inflation</i>			
Consumer Price Index (CPI)*	CPIAUCSL	$\Delta^2 \log(x)$	✓
Consumer Price Index Less Food and Energy*	CPILFESL	$\Delta^2 \log(x)$	
PCE: Chain-type Price Index*	PCEPI	$\Delta^2 \log(x)$	
PCE Excluding Food and Energy*	PCEPILFE	$\Delta^2 \log(x)$	
PCE: Food*	DFXARC1M027SBEA	$\Delta^2 \log(x)$	
PCE: Energy goods and services*	DNRGRC1M027SBEA	$\Delta^2 \log(x)$	
Producer Price Index by Commodity: All Commodities	PPIACO	$\Delta^2 \log(x)$	

Note: Series marked with an asterisk (\*) are seasonally adjusted. A checkmark (✓) indicates the variable is included in the reduced set.

Table 10: Quarterly Macroeconomic Data Series

Series Name	Code	Transformation	Reduced Set
<i>Aggregate Economic Activity</i>			
Gross Domestic Product*	GDP	$\Delta \log(x)$	✓
<i>Labor Market</i>			
Nonfarm Business Sector: Unit Labor Costs*	ULCNFB	$\Delta \log(x)$	

Note: Series marked with an asterisk (\*) are seasonally adjusted. A checkmark (✓) indicates the variable is included in the reduced set.

# E Macroeconomic Results

## E.1 Plots

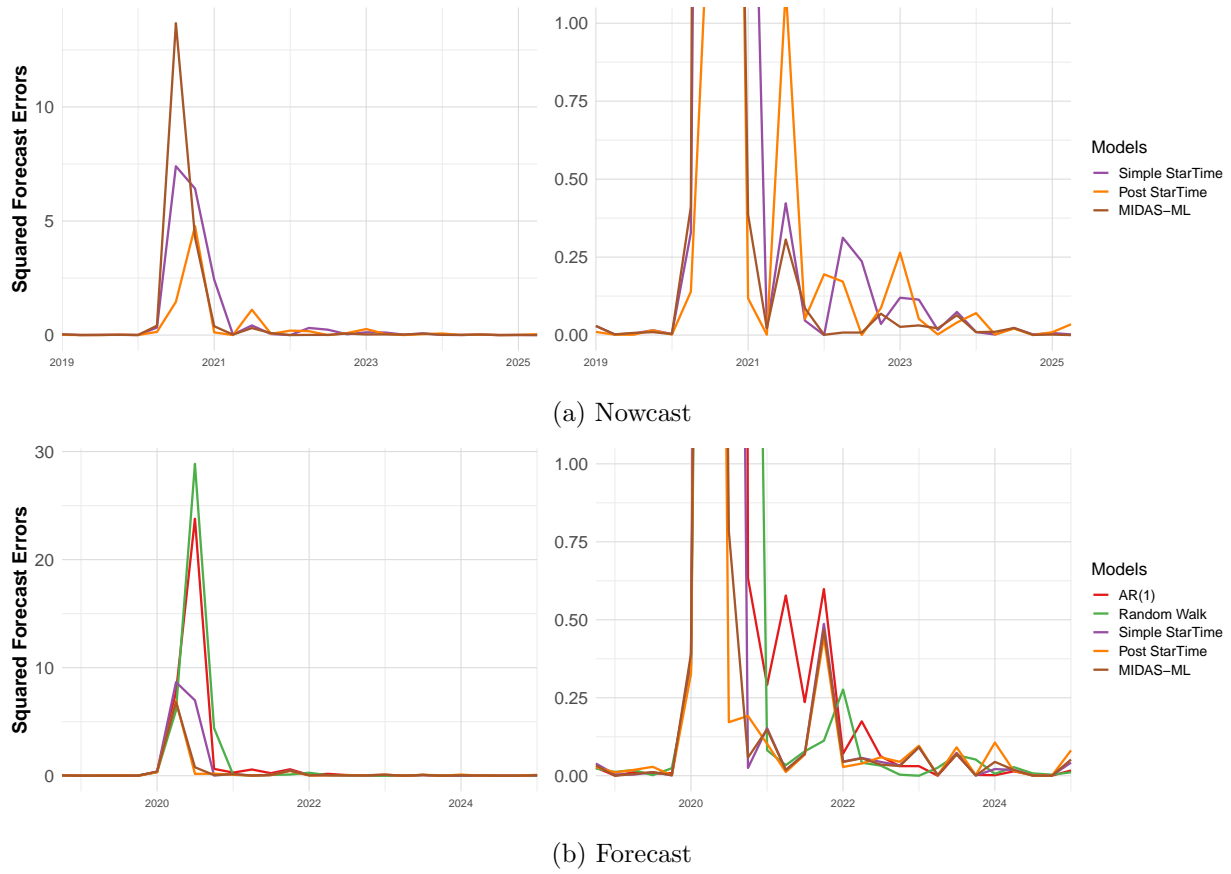
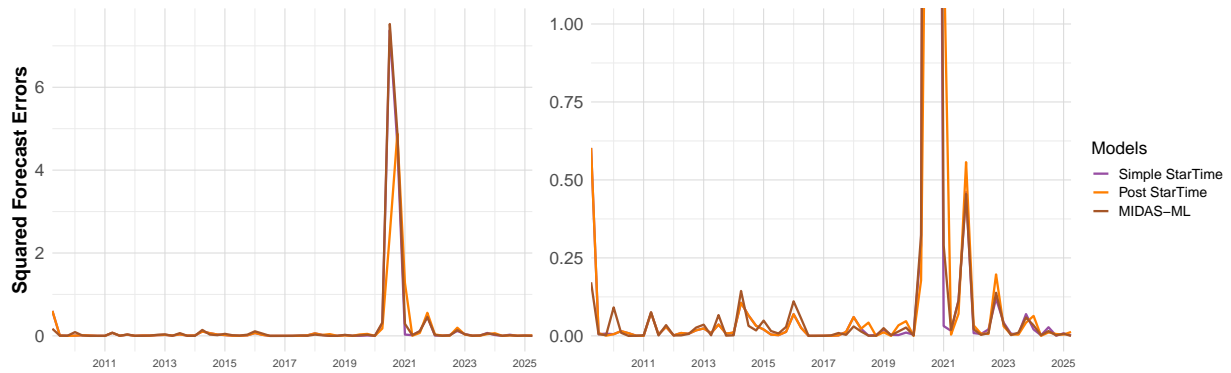
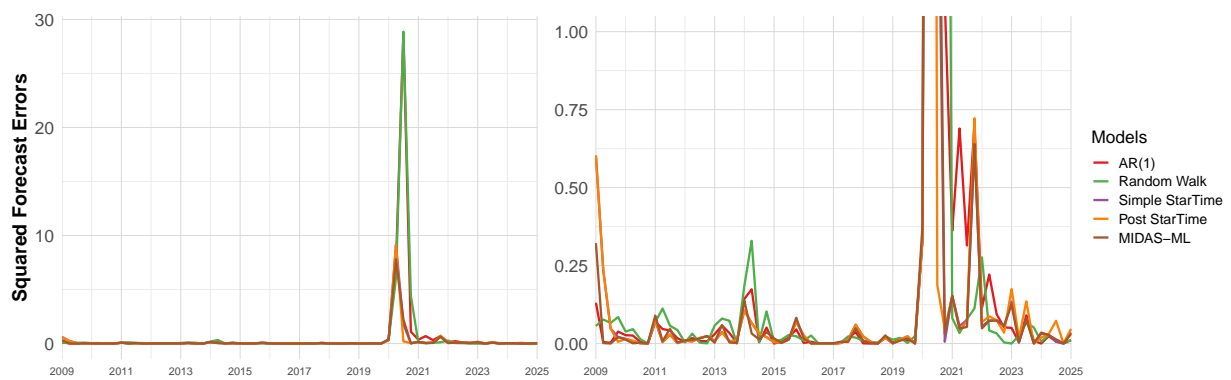


Figure 10: Evolution of the squared forecast errors for the Full Set (398 predictors) with  $W = 105$ . Both (a) and (b) include a censored zoom to account for COVID-19 volatility. The plotted squared forecast errors values are multiplied by 1000.

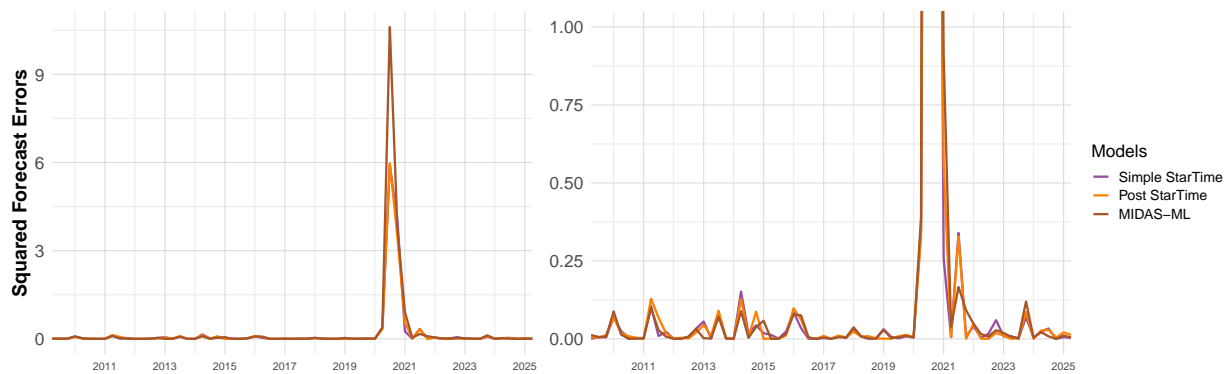


(a) Nowcast

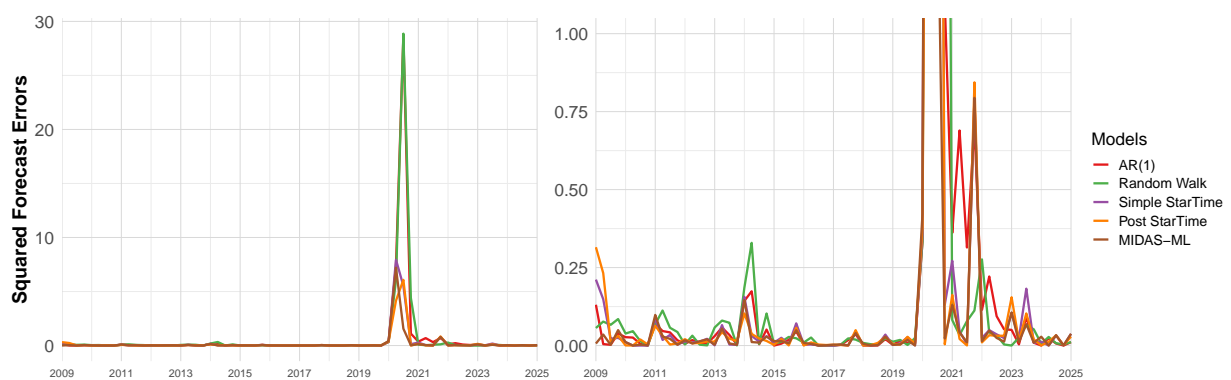


(b) Forecast

Figure 11: Evolution of the squared forecast errors for the Full Set (398 predictors) with  $W = 66$ . Both (a) and (b) include a censored zoom to account for COVID-19 volatility. The plotted squared forecast errors values are multiplied by 1000.



(a) Nowcast



(b) Forecast

Figure 12: Evolution of the squared forecast errors for the Reduced Set (49 predictors) with  $W = 66$ . Both (a) and (b) include a censored zoom to account for COVID-19 volatility. The plotted squared forecast errors values are multiplied by 1000.

## E.2 Tables

Table 11: MSFE for window  $W = 66$

	Post StarTime		Simple StarTime		MIDAS-ML		AR(1)	Random walk
	$h = 0$	$h = 1$	$h = 0$	$h = 1$	$h = 0$	$h = 1$		
<i>Reduced Set</i>								
Total	0.184	0.206	0.186	0.258	0.264	0.175	0.637	0.651
Non-peak	0.021	0.031	0.020	0.030	0.019	0.021	0.032	0.041
COVID-Peak	1.342	1.456	1.367	1.884	2.005	1.272	4.947	4.994
<i>Full Set</i>								
Total	0.174	0.202	0.225	0.222	0.232	0.200	0.637	0.651
Non-peak	0.032	0.042	0.030	0.039	0.025	0.029	0.032	0.041
COVID-Peak	1.183	1.338	1.614	1.526	1.706	1.418	4.947	4.994

*Note: MSFE values are multiplied by 1000 due to the small scale of GDP growth.*

Table 12: Model Confidence Set  $p$ -values:  $T_{max}$  (Total,  $W = 105$ )

Configuration			Models				
Reduction	Window	Horizon	Post StarTime	Simple StarTime	MIDAS-ML	AR(1)	Random Walk
Full	105	0	1.000	0.167	0.752		
Full	105	1	1.000	0.670	1.000		
Reduced	105	0	1.000	1.000	1.000		
Reduced	105	1	1.000	1.000	1.000		
Univariate Benchmark						0.537	0.632

*Note: Values represent  $p$ -values for the Model Confidence Set (MCS) using the  $T_{max}$  statistic.  $p$ -values  $\geq 0.05$  indicate inclusion in the MCS.*

Table 13: Model Confidence Set  $p$ -values:  $T_{max}$  (Non-Peak,  $W = 105$ )

Configuration			Models				
Reduction	Window	Horizon	Post StarTime	Simple StarTime	MIDAS-ML	AR(1)	Random Walk
Full	105	0	0.545	0.517	1.000		
Full	105	1	0.257	1.000	1.000		
Reduced	105	0	1.000	1.000	1.000		
Reduced	105	1	1.000	1.000	1.000		
Univariate Benchmark						0.998	0.934

*Note: Values represent  $p$ -values for the Model Confidence Set (MCS) using the  $T_{max}$  statistic.  $p$ -values  $\geq 0.05$  indicate inclusion in the MCS.*

Table 14: Model Confidence Set P-Values:  $T_{max}$  (Total,  $W = 66$ )

Configuration			Models					
Reduction	Window	Horizon	Post StarTime	Simple StarTime	MIDAS-ML	AR(1)	Random Walk	
Full	66	0	1.000	1.000	1.000			
Full	66	1	1.000	1.000	1.000			
Reduced	66	0	1.000	1.000	1.000			
Reduced	66	1	1.000	1.000	1.000			
Univariate Benchmark						0.537	0.553	

*Note: Values represent p-values for the Model Confidence Set (MCS) using the  $T_{max}$  statistic. p-values  $\geq 0.05$  indicate inclusion in the MCS.*

Table 15: Model Confidence Set P-Values:  $T_{max}$  (Non-Peak,  $W = 66$ )

Configuration			Models					
Reduction	Window	Horizon	Post StarTime	Simple StarTime	MIDAS-ML	AR(1)	Random Walk	
Full	66	0	1.000	1.000	1.000			
Full	66	1	0.827	0.938	1.000			
Reduced	66	0	1.000	1.000	1.000			
Reduced	66	1	1.000	1.000	1.000			
Univariate Benchmark						1.000	0.611	

*Note: Values represent p-values for the Model Confidence Set (MCS) using the  $T_{max}$  statistic. p-values  $\geq 0.05$  indicate inclusion in the MCS.*